Energy & Environmental Science

ROYAL SOCIETY OF CHEMISTRY

REVIEW

View Article Online
View Journal | View Issue

Cite this: *Energy Environ. Sci.*, 2022, **15**, 550

Liquid electrolyte development for low-temperature lithium-ion batteries

Dion Hubble,[a] David Emory Brown,[ab] Yangzhi Zhao,[a] Chen Fang,[a] Jonathan Lau,[a] Bryan D. McCloskey[b] and Gao Liu*[a]

Received 11th June 2021,
Accepted 10th November 2021

DOI: 10.1039/d1ee01789f

rsc.li/ees

Lithium-ion batteries (LIBs) power virtually all modern portable devices and electric vehicles, and their ubiquity continues to grow. With increasing applications, however, come increasing challenges, especially when operating conditions deviate from room temperature. While high-temperature performance and degradation has been extensively studied in LIBs, sub-zero Celsius performance has received less attention, despite being critical for batteries in transportation roles. Although many individual processes contribute to the capacity loss commonly observed in LIBs at low temperatures, most of them are governed to some extent by the non-aqueous liquid electrolyte present throughout the cell interior. Therefore, electrolyte engineering presents an unparalleled opportunity to study and address the fundamental causes of low-temperature failure. In this review, we first briefly cover the various processes that determine lithium-ion performance below 0 °C. Then, we outline recent literature on electrolyte-based strategies to improve said performance, including various additives, solvents and lithium salts. Finally, we summarize these findings and provide some perspectives on the current state of the field, including promising new areas of investigation.

Broader context

The upcoming switch to renewable energy across the globe will depend heavily on lightweight, reliable energy storage being readily available. As of now, the best candidate for the job is the lithium-ion battery (LIB). Nearly all portable electronics and electric vehicles already contain lithium-ion chemistry in some form, and LIBs have garnered serious consideration for expanded roles in aerospace and power distribution. However, as their applications increase in significance, so too do their drawbacks, including their notorious temperature sensitivity. LIB operating characteristics at elevated temperatures (>40 °C) have been extensively studied, but low-temperature (<0 °C) performance has received much less attention, despite its increasing relevance. For example, widespread adoption of electric vehicles will require them to function during winter just as reliably as during summer. In the course of our research, we have found that LIB operation at low temperature is often governed most strongly by electrolyte composition. Therefore, we present this review on liquid electrolyte design for LIBs under low-temperature conditions. It is our hope that this article will inspire additional advancements in the field so that clean energy will become available to more people in more environments than ever before.

Introduction

It is difficult to overstate how thoroughly the lithium-ion battery, or LIB, has permeated life in the 21st century thus far. At the time of this writing, nearly all portable electronics and electric vehicles contain some form of LIB, and more recently they have garnered serious consideration for expanded roles in aerospace[1] and power distribution.[2,3] However, as their applications increase in significance, so too do their drawbacks, including their notorious temperature sensitivity. LIBs function acceptably between 0–40 °C, but they encounter severe problems under harsher conditions.[4–6] Performance beyond the high end of this range has been extensively studied, including the mechanisms of high-temperature battery degradation and its consequences, ranging from capacity fade to thermal runaway.[7,8] By comparison, the low-temperature performance of LIBs has received considerably less attention, especially in the preceding 15 years. Nonetheless, this topic continues to gain relevance, as emerging applications in energy storage require increasing tolerance to frigid conditions. For example, widespread adoption of electric vehicles will require them to function during winter just as reliably as during summer.

Successful LIB operation depends on a complex web of physical and chemical processes that must function harmoniously; as a

[a] *Energy Storage and Distributed Resources Division, Lawrence Berkeley National Laboratory, 1 Cyclotron Road, Berkeley, CA 94720, USA. E-mail: gliu@lbl.gov*
[b] *Department of Chemical and Biomolecular Engineering, University of California, Berkeley, CA 94720, USA*

result, it is hardly possible to change one aspect of battery design without affecting many others. This is especially true for the non-aqueous liquid electrolytes used in LIBs, which contact nearly all internal surface area. Indeed, the early success of lithium-ion chemistry was spurred by the discovery that ethylene carbonate (EC) can form a dimensionally-stable solid electrolyte interphase (SEI) on carbon when included as an electrolyte co-solvent.[9] On the other hand, organic electrolyte chemistry may also contribute to capacity loss,[10] poor power density[11] and flammability,[12] among other concerns. Therefore, the prudent battery scientist should view electrolyte design as a ''double-edged sword'' with the potential to address multiple points of failure, but conversely introduce multiple new complications.

In light of its key role in LIB function, it should be unsurprising that early studies identified electrolyte chemistry as one of the main governing factors in low-temperature performance,[13] a consensus that largely remains to this day. In an effort to inspire renewed research in this area, we hereby present this concise review of liquid electrolyte design for low-temperature LIBs. We first summarize the various major processes that determine lithium-ion performance metrics at low temperature (<0 °C) and how the electrolyte may influence them. Then, we review research geared towards improving low-temperature performance using electrolyte engineering (additives, solvents and salts; Fig. 1), focusing primarily on recent reports (2010–now). While the majority of this work covers LIBs with traditional active materials – graphite (Gr) or $Li_4Ti_5O_{12}$ (LTO) anodes plus lithium transition–metal oxide or phosphate cathodes – we also include a brief summary of reports related to silicon anodes at low temperature, since this material is a likely candidate for next-generation commercial LIBs. Finally, we conclude with some suggestions as to future directions of this field.

Dion Hubble

Dion Hubble received his PhD (2019) and Master's (2016) degrees in Molecular Engineering from the University of Washington subsequent to his Bachelor's (2014) degree in Chemical Engineering from Texas A&M University. He joined Lawrence Berkeley National Laboratory in 2020 as a postdoctoral scholar under the supervision of Dr Gao Liu. His research interests center on the design, synthesis, and integration of polymers/organic materials into devices or processes for energy-related applications.

David Emory Brown

David E. Brown received his BS in chemical engineering in 2017 from Columbia University. He is currently a PhD candidate and NSF Graduate Research Fellow in Prof. Bryan McCloskey's research group at the University of California, Berkeley and the Lawrence Berkeley National Laboratory. His research interests focus on Li plating detection during extreme fast charging of graphite electrodes in Li-ion batteries and on electrolyte engineering to improve Li-ion battery low temperature performance.

Chen Fang

Chen Fang received his PhD degree in Chemistry from Brown University in 2018. His research was in the areas of organic synthesis, self-assembled monolayers and bottom-up fabrication. In 2019, he started to work as a postdoctoral researcher at Lawrence Berkeley National Laboratory. His current research activities include electrolyte and binder materials for advanced rechargeable batteries, surface and interface chemistry inside lithium-ion batteries, and solid-state batteries.

Bryan D. McCloskey

Bryan D. McCloskey is an Associate Professor and the Vice Chair of Graduate Education in the Department of Chemical and Biomolecular Engineering at the University of California, Berkeley, and also holds a joint appointment as a Faculty Engineer in the Energy Storage and Distributed Resources Division at Lawrence Berkeley National Laboratory. His laboratory currently focuses on a variety of challenges facing Li-ion and metal–air batteries, including high voltage cathode stability, advanced cathode material development, extreme fast charging, low temperature electrolyte formulations, and polyelectrolyte solution transport phenomena. More information about the McCloskey Lab can be found at the Lab's website: www.mccloskeylab.com.

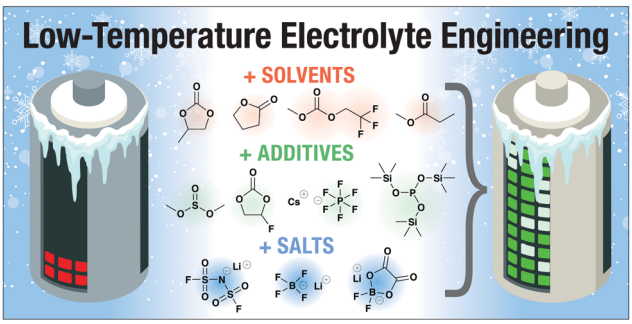

Fig. 1 Schematic of electrolyte engineering strategies for improved low-temperature performance. A typical LIB electrolyte contains lithium hexafluorophosphate dissolved in a mixture of ethylene carbonate and linear carbonates. However, incorporation of non-traditional solvents (top row, from left: propylene carbonate, gamma-butyrolactone, methyl [3,3,3-trifluoroethyl] carbonate, methyl propionate), additives (middle row, from left: dimethyl sulfite, fluoroethylene carbonate, cesium hexafluorophosphate, tris[trimethylsilyl]phosphite) and/or salts (bottom row, from left: lithium bis[fluorosulfonyl]imide, lithium tetrafluoroborate, lithium difluoro[oxolato]borate) can dramatically improve available capacity below 0 °C.

Challenges in low-temperature LIB performance

While the processes that limit low-temperature LIB performance are myriad, their effect is commonly the same: capacity loss. The usable capacity of a fresh lithium–ion cell between predefined voltage limits generally decreases with decreasing temperature – especially below −20 °C – sometimes to less than 25% of its room-temperature value. This capacity loss is usually reversible when the temperature is raised back to normal conditions. On the other hand, irreversible capacity loss may also occur if the cell is charged at low temperature, due to the plating of lithium metal on the anode surface, which is only partially recoverable.[14] Both types of capacity loss may be largely attributed to increased internal resistance of the cell at sub-zero temperatures. This internal resistance has many components, each corresponding to a different physical process associated with Li^+ transport across the cell (Fig. 2).[15] Electrolyte composition can affect many of these processes, as we discuss below.

Gao Liu

Gao Liu is a Senior Scientist and Group Leader of the Applied Energy Materials Group in the Energy Storage and Distributed Resources Division at Lawrence Berkeley National Laboratory. His laboratory combines synthetic chemistry, composite engineering and electrochemistry to solve interdisciplinary problems. Liu Lab's current research in battery and energy storage include silicon materials and electrode binders for advanced lithium-ion battery, lithium-sulfur battery, solid-state battery, and electrode interfaces. His lab also performs research in hydrogen generation, plastic recycling, and advanced manufacturing. More information about the Liu Lab can be found at the Lab's website: https://liulab.lbl.gov.

Bulk electrolyte considerations

Conductivity. A typical LIB electrolyte contains anywhere from 0.8 M to 1.5 M $LiPF_6$ in a solvent mixture of organic carbonates, one of which is ethylene carbonate (EC). This compound is favored for many reasons, including its large dielectric permittivity (ε = 90 at 40 °C),[16] which enables strong dissociation of Li^+ and PF_6^- to form highly conductive solutions. Most of all, however, EC is prized for its unique ability to form a protective SEI layer on graphite upon its decomposition at low potentials.[13] On the other hand, the melting point of EC (36 °C)[17] is well above the operating temperature of most LIBs. Therefore, it is generally blended with 50–70% of a linear carbonate (*e.g.*, dimethyl carbonate [DMC], diethyl carbonate [DEC] and/or ethyl methyl carbonate [EMC]) to widen the working temperature range and lower the viscosity, which improves conductivity per the Stokes–Einstein and Nernst–Einstein relations. In particular, $LiPF_6$/EC/EMC electrolytes have been well-characterized across a large range of compositions and ambient conditions; the conductivity of a typical blend is 5–10 mS cm^{-1} at room temperature.[18]

Within the operating range of LIBs, electrolytic conductivity universally decreases with temperature – a trend primarily attributable to viscosity effects. Naturally, this causes the internal resistance to rise. Because viscosity correlates with EC content, it is generally accepted that this solvent should be minimized in cells designed for low temperature; however, this task has proven challenging due to the vital role of EC in low-resistance and stable SEI formation, causing lean-EC electrolytes to commonly suffer from reduced cycling stability and Coulombic efficiency. Additionally, bulk ohmic resistance is rarely the largest component of total battery impedance,† meaning that conductivity alone does not typically predict low-temperature performance with any degree of accuracy.

Liquidus point. Perhaps the most important reason to minimize EC content in low temperature LIB electrolytes is not viscosity, but crystallization tendency. Because of this solvent's high melting point, even its concentrated electrolyte solutions tend to solidify easily. Blending with lower-melting carbonates can decrease the melting point somewhat, but nonetheless the liquidus point (where solids first appear during cooling) of the common EC/EMC system remains above 0 °C for concentrations >30 mol% EC (Fig. 3a).[19] Freezing point depression through the addition of lithium salt (1 M $LiPF_6$) further lowers the liquidus to −20 to −30 °C for practical electrolytes,[19–21] which may partially explain why this

† An important exception may be found in large-format cells at high discharge rates, where poor Li^+ diffusivity can cause localized high- or low-concentration hotspots which dominate behavior (see ref. 60).

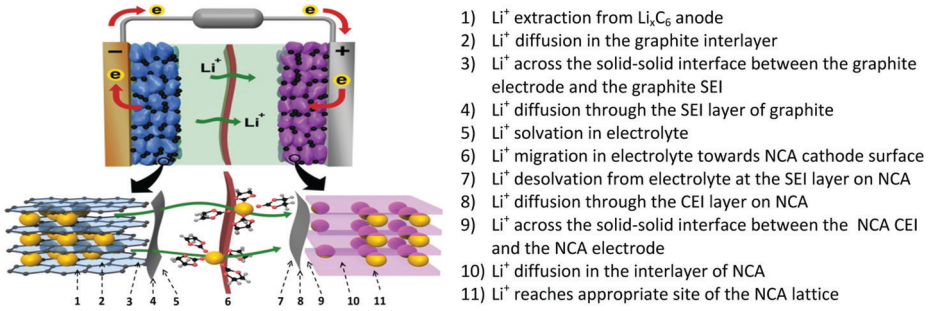

Fig. 2 Complete overview of lithium transport pathway in a graphite‖$LiNi_{0.80}Co_{0.15}Al_{0.05}O_2$ full cell. The identity of the rate-limiting step may change with temperature, depending on the active material properties and electrolyte composition. Reprinted with permission from ref. 15. Copyright 2017 American Chemical Society.

temperature range is generally considered a "turning point" for capacity loss in LIBs. As compared to linear carbonates, the structurally-related molecule propylene carbonate (PC) suppresses EC crystallization more effectively when added as a cosolvent (Fig. 3b). PC is quite popular as a low-temperature solvent component for this reason among several others (see the relevant section below). Generally speaking, when crystallization of EC does occur, it lowers the conductivity of the remaining liquid phase and may even block electrode pores, temporarily isolating sections of active material. Both effects cause capacity loss and are therefore critical to avoid.

Transference number. One additional aspect of low-temperature electrolyte design that has been mostly overlooked is the thermal dependence of Li^+ transference number (t_+). This parameter describes the fraction of current attributable to movement of Li^+, as opposed to its counterion, and is directly linked to polarization resistance in working batteries[22,23] as well as lithium dendrite growth.[24] While simple in concept, this parameter is difficult to accurately measure for non-dilute electrolytes, and is usually determined at room temperature only ($t_+ \approx 0.3$–0.5 for typical formulations).[25,26] Nonetheless, recent work by Landesfeind and Gasteiger,[27] among others,[28–30] indicates that t_+ may decrease with decreasing temperature for typical LIBs electrolytes. The resulting increase in polarization could contribute to premature voltage drop, which is often observed during low temperature discharge. While the

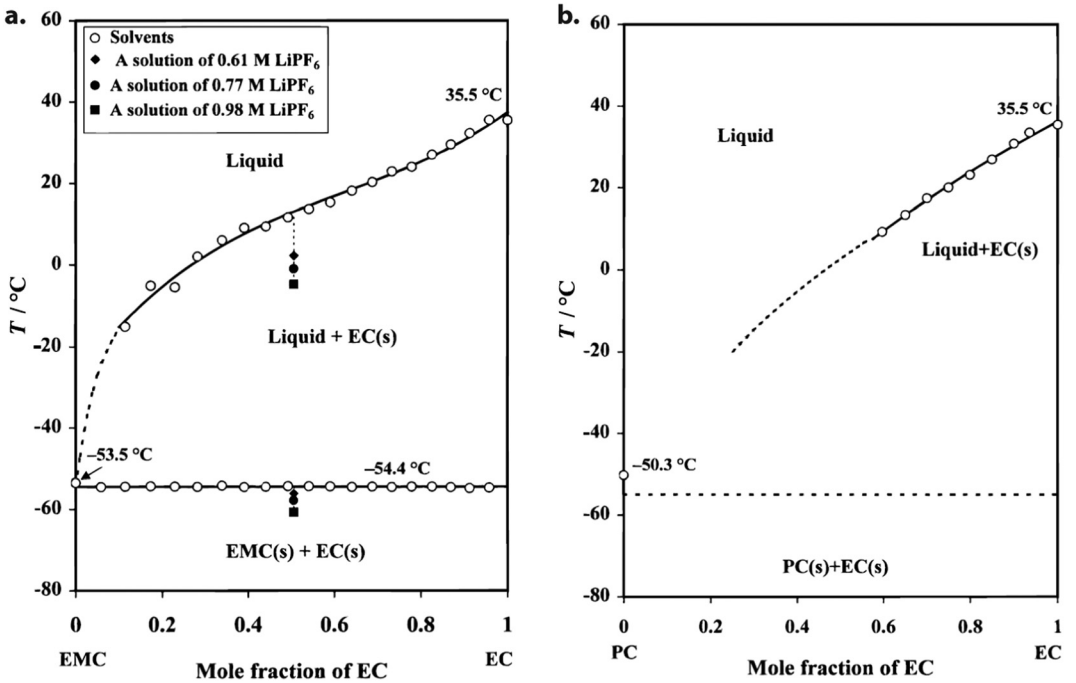

Fig. 3 (a) Liquid–solid phase diagram of EMC-EC. The open dots represent measured data from which the solubility curve and the solidus line have been obtained through data fitting. The dotted curve is an estimated extension of the measured liquidus curve. The closed dots represent measured data for three different solutions of $LiPF_6$ in an EMC-EC solvent, plotted to demonstrate the change of the phase transition temperatures with the concentration of a lithium salt. (b) Liquid–solid phase diagram of PC–EC. The dotted solubility curve and the solidus line are both estimated due to the tendency of PC-rich mixtures to supercool, precluding accurate measurement. Compared to EMC, PC reduces liquidus temperature more effectively when present >20 mol% in the mixture. Reprinted from ref. 19, copyright The Electrochemical Society. Reproduced by permission of IOP Publishing Ltd. All rights reserved.

mechanistic underpinnings of this parameter's temperature dependence have yet to be clarified, Landesfeind and Gasteiger suggest that large hydrodynamic volume of (solvated) Li^+ relative to PF_6^- may play a role, as well as increased formation of ion aggregates like $[Li(PF_6)_2]^-$. This topic deserves further experimental and computational exploration in order to determine the precise role that t_+ plays in low-temperature performance characteristics.

Interfacial considerations

Charge transfer resistance. At this time, it is widely accepted that electrolyte/active material interfacial processes make up the bulk of LIB impedance below freezing, although the exact identity of these processes remains an active subject of research. Early impedance studies hinted towards a kinetic origin for the limiting resistance, as work by Zhang, Xu and Jow[31] revealed a strong dependence of LIB overpotential on state-of-charge, especially below −20 °C (Fig. 4a). Furthermore, impedance spectra showed increasing dominance of a mid-frequency component as temperature decreased, a region generally assigned to charge transfer resistance (R_{ct}). However, the exact physical meaning of this term is often ambiguous, as "charge transfer" may itself consist of multiple, reaction-dependent steps. Furthermore, these processes are likely to generate different resistances at either electrode, which this experiment did not distinguish between. These authors' follow-up work noted an Arrhenius-type relationship between R_{ct} and temperature (Fig. 4b), and that the activation energy of the charge transfer process ($E_{a,ct}$) was strongly dependent on electrolyte composition (both salt and solvent).[32] This $E_{a,ct}$ term varied independently from bulk ion transport resistance. Furthermore, Abraham *et al.* identified near-identical $E_{a,ct}$ trends for binder-and-carbon-free LTO|$LiMn_2O_4$ cells, despite the absence of any significant interphase on these materials.[33] Taken together, these results led the authors to strongly suggest Li^+ desolvation as the rate-limiting process associated with charge transfer, as opposed to transport through an SEI or across the SEI-active material boundary.

Recent works by various authors have strengthened the conclusion that Li^+ desolvation is the rate-limiting process at low temperature (Fig. 5a). Xu and coworkers corroborated previous results by demonstrating that $E_{a,ct}$ on LTO varies with the electron donicity of the solvent, which is a major factor in solvation strength. These authors obtained values of 40 kJ mol^{-1} for 1 M LiTFSI in tetrahydrofuran *vs.* 52.5 kJ mol^{-1} for 1 M $LiPF_6$ in EC/EMC 3 : 7.[34] Their report also noted similar resistance trends on graphite anodes, but with values consistently offset upwards by ~20 kJ mol^{-1}; the authors attributed this to the additional effect of ion transport through a resistive SEI, which appeared at a similar resonant frequency and was difficult to separate out. Similarly, Li *et al.* studied Li‖Gr and Li‖$LiFePO_4$ half cells with identical electrolytes, finding graphite to be limiting in both charge transfer and interfacial transport (although electrolyte design had a strong effect).[35]

In 2017, a team from Pacific Northwest National Laboratory systematically compared carbonate electrolytes of varying

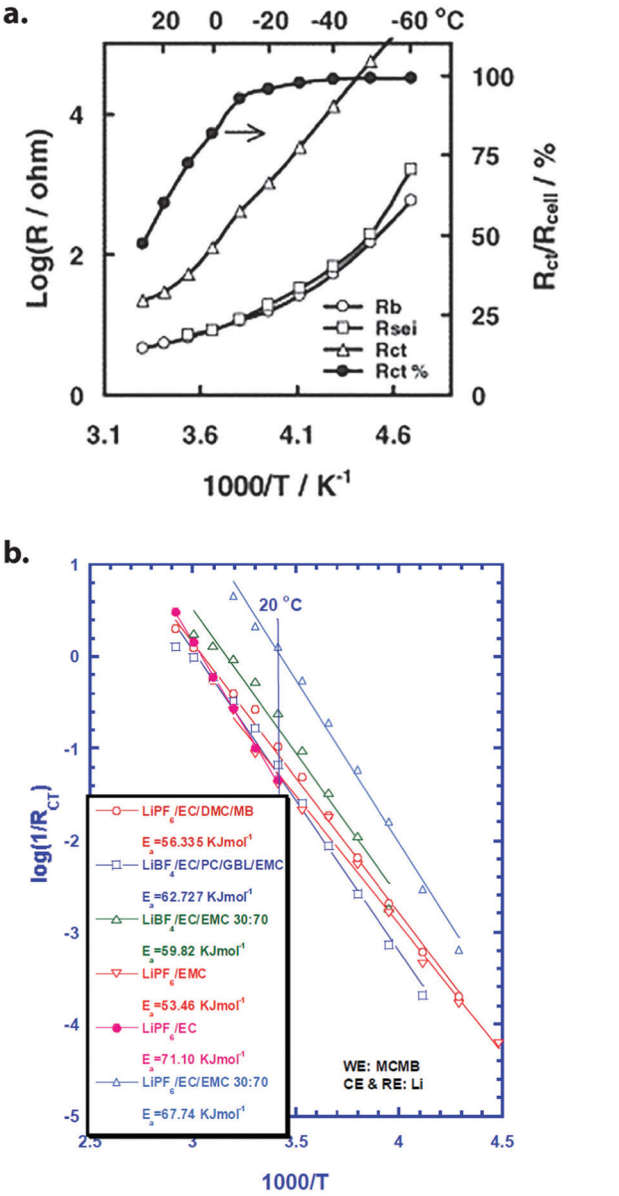

Fig. 4 (a) Variation of bulk electrolyte resistance (R_b), SEI resistance (R_{SEI}), charge-transfer resistance (R_{ct}) and the percentage of total resistance made up of R_{ct} (R_{ct}%) with temperature in a commercial Li-ion cell discharged to 3.87 V. Reprinted from ref. 31 with permission from Elsevier. (b) Arrhenius plot of R_{ct} *vs.* temperature for Li‖MCMB half cells with varying electrolytes. Extracted E_a values (kJ mol^{-1}) are included in the legend. Reprinted from ref. 32, copyright The Electrochemical Society. Reproduced by permission of IOP Publishing Ltd. All rights reserved.

composition in Gr‖Gr, NCA‖NCA and LTO‖LTO symmetric cells, thereby eliminating any competing effects from Li metal or multiple electrodes.[15] Despite the disparate chemical structures of these materials and their interfaces, their mid-frequency EIS responses were nearly identical at −40 °C, implying that ion desolvation – their only common factor – is the rate-limiting process in each case. Furthermore, when graphite anodes were subjected to an SEI-formation process in one electrolyte, then re-assembled into Gr‖NCA full cells with another electrolyte, the discharge capacity of the cells at

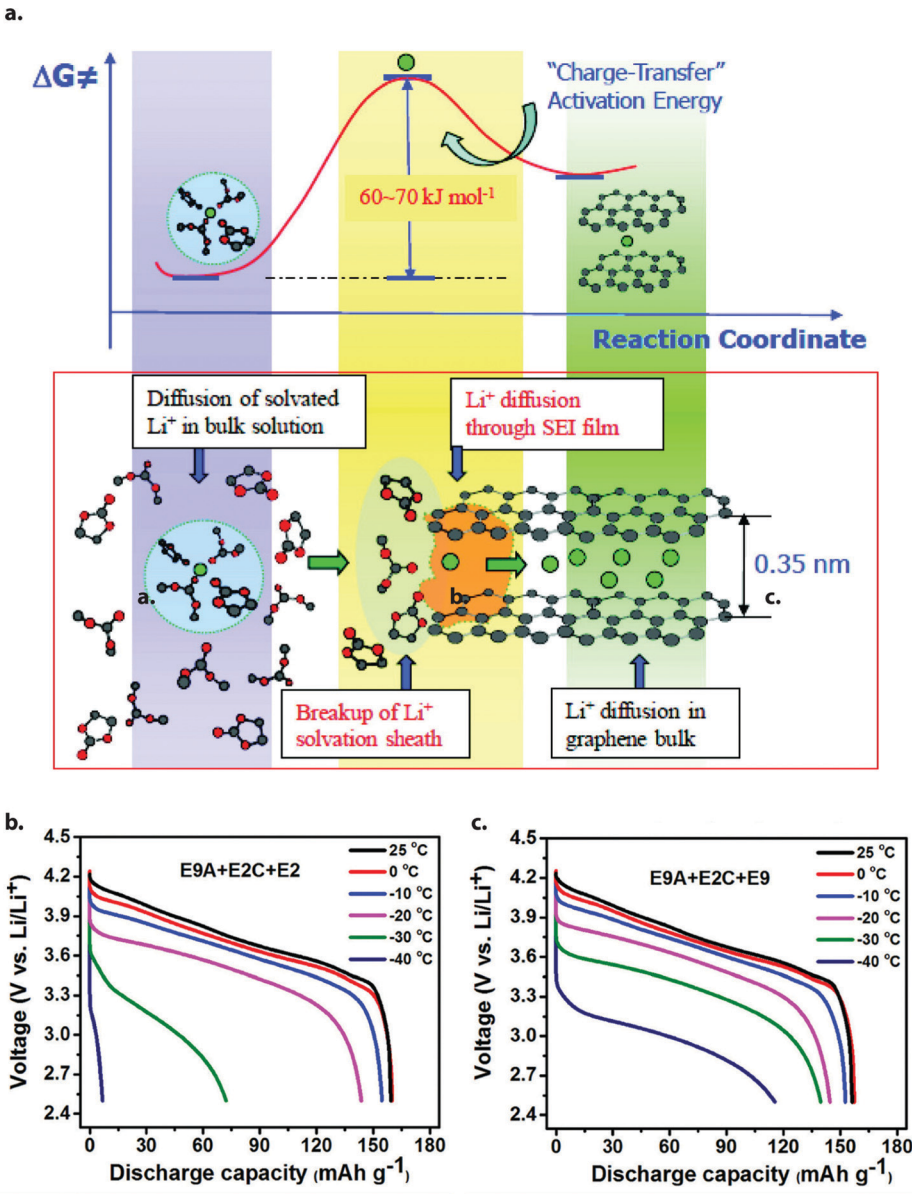

Fig. 5 (a) Schematic depicting Li^+ desolvation at the graphite interface, widely proposed to be the rate-limiting step in charge transfer at low temperature. Reprinted with permission from ref. 34. Copyright 2010 American Chemical Society. (b and c) Discharge profiles of Gr‖NCA cells containing identical pre-cycled electrodes, but different electrolytes. E9A refers to an anode that has undergone formation cycles in E9 electrolyte (an EC-lean formulation), while E2C refers to a cathode that has undergone formation in E2 (an EC-rich formulation). Despite identical pre-formed interphase layers, major differences in discharge capacity below −20 °C are observed, consistent with lower R_{ct} in the EC-lean electrolyte E9. Reprinted/adapted with permission from ref. 15. Copyright 2017 American Chemical Society.

−20 °C had virtually no correlation with the former electrolyte composition, but correlated strongly with the latter (Fig. 5b and c). The overall lesson appears to be that electrolyte design affects low temperature performance primarily by determining the makeup of Li-ion solvation shells – the breakup of which requires the greatest energy input out of all simultaneous processes during operation.

Solid–electrolyte interphase resistance. The additional major impact of electrolyte (on graphite especially, but also on >4 V cathode materials) is that of interphase composition. Interphase layers may form on either anode (SEI) or cathode (CEI) surfaces, and they contribute a bulk transport resistance (R_{SEI}) to cell impedance, which can vary in magnitude from inconsequential to nearly as large as R_{ct}.[36] In fact, some early research pointed to SEI conductivity as the main limiting factor in low-temperature LIB capacity,[37] a common misconception that remains to this day. Of course, as discussed above, we now know that R_{SEI} is unlikely to be the largest component of internal resistance below 0 °C, at least for "typical" cell designs, *i.e.* a graphite anode, oxide cathode and EC-based electrolyte.

Why, then, does this misconception persist? One likely reason is that R_{SEI} and R_{ct} can be difficult to distinguish.

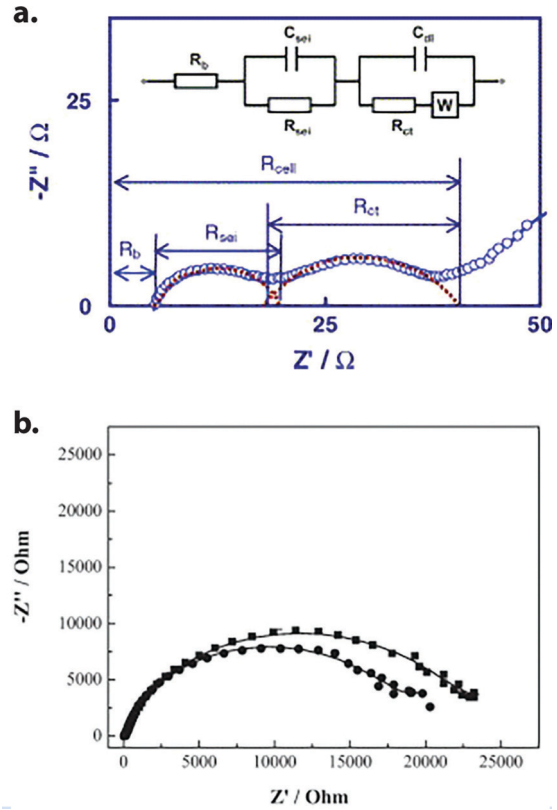

Fig. 6 (a) Nyquist plot of Li-ion cell impedance showing relatively well-separated semicircles. In this case, both the individual values of R_{SEI} and R_{ct} can be reasonably determined (although they each represent lumped values for cathode and anode processed). Reprinted from ref. 31 with permission from Elsevier. (b) Nyquist plot of Li‖MCMB half-cell impedance, where only one semicircle is distinguishable. In this case R_{SEI} cannot be separated from R_{ct}, either due to similar time constants for both processes or because one is much larger than the other. Additional context is required to interpret the combined "interfacial resistance." Reprinted from ref. 66 with permission from Elsevier.

The impedances associated with interphase ion transport and charge transfer often overlap quite substantially in characteristic frequency, which can cause them to appear as a single semicircle in Nyquist plots generated by EIS (Fig. 6a and b). Attempting to extract separate, accurate resistance values from such a feature becomes an exercise in futility, and it is easier to refer to a single, combined value for "interfacial resistance." Another possible reason is that R_{SEI}, while not the largest component of total resistance, may still compose a sufficient fraction of it to notably affect performance. An excellent example of this can be found in the recent work of Liu *et al.*, who systematically studied interphase-forming additives, while keeping the base electrolyte constant.[38] Under such conditions, R_{ct} should hardly change, but capacity improvements of up to 7% were observed at −40 °C and C/5 rate, which correlated well to changes in interphase chemistry/thickness with different additives.

The third possible answer is that interfacial chemistry may not be totally separable from charge-transfer kinetics. After all, if Li^+ desolvation at the electrolyte/interphase boundary is responsible for R_{ct}, it follows that surface chemistry may play a role in that process – partially coordinating the ion as its solvation shell strips away, for example. However, such an effect would be very difficult to study, especially given how little we still know about SEI/CEI chemistry on the molecular scale, which is notoriously difficult to characterize.[39–41] Nonetheless, the fact remains that changes to SEI composition are often reported to produce outsized effects on low-temperature capacity (*vide infra*). Therefore, when posed the question "Exactly what role does SEI/CEI play in low-temperature performance?", we can unfortunately provide no definitive answer other than "It depends."

That being said, even if R_{SEI} does not ordinarily limit low-temperature capacity, the stabilizing role of the interphase cannot be ignored. In order to successfully cycle a graphite-based LIB at any temperature, the electrolyte must form a dimensionally-stable layer to protect against continued decomposition, as well as exfoliation. Therefore, the issue is often less about optimizing interphase composition for sub-freezing performance directly, and more about adjusting other factors (freezing point, charge transfer resistance, *etc.*) without compromising the robustness of anode/cathode interphases. This is of special concern for low-liquidus-point electrolytes with little-to-no EC content, which must rely on additives for stable cycling.

Lithium plating

Our discussion thus far has centered on discharge capacity as the primary metric by which low-temperature performance is measured, with the implicit assumption that charging is done at 25 °C or higher. This is because charging a graphite-anode LIB at lower than 25 °C and/or at a high rate introduces significant risk of lithium metal plating, a major safety hazard and cause of premature capacity fade. Much of the work to detect the onset of – and to mitigate – lithium metal deposition on graphite anodes has focused on achieving fifteen-minute charge times at room temperature. This has been well summarized and described in other reviews, including Waldman *et al.*,[42] Liu *et al.*[43] and Tomaszewska *et al.*;[11] the latter review also includes some analysis of work to enable low-temperature LIB operation. While "extreme fast charging" at around 25 °C has numerous issues, low-temperature charging brings many similar challenges associated with undesired lithium metal nucleation and growth, even at relatively slow charging rates.

During "typical," facile charging of a graphite-anode LIB, Li^+ ions are reduced at the graphite anode and intercalate between individual graphene layers. However, if the electrochemical potential of the graphite particle dips below 0 V *vs.* Li/Li^+, lithium metal formation becomes thermodynamically possible. Graphite is particularly susceptible to this phenomenon because its operating potential (under open-circuit conditions) is only ~100 mV *vs.* Li/Li^+.[44] When current is applied, anode potential may further drop into the lithium plating regime, given sufficiently-large overpotential at the graphite/electrolyte interface (Fig. 7a). As discussed above, detrimental overpotentials can arise from a number of factors, including ohmic losses—which scale with applied charging current—as well as

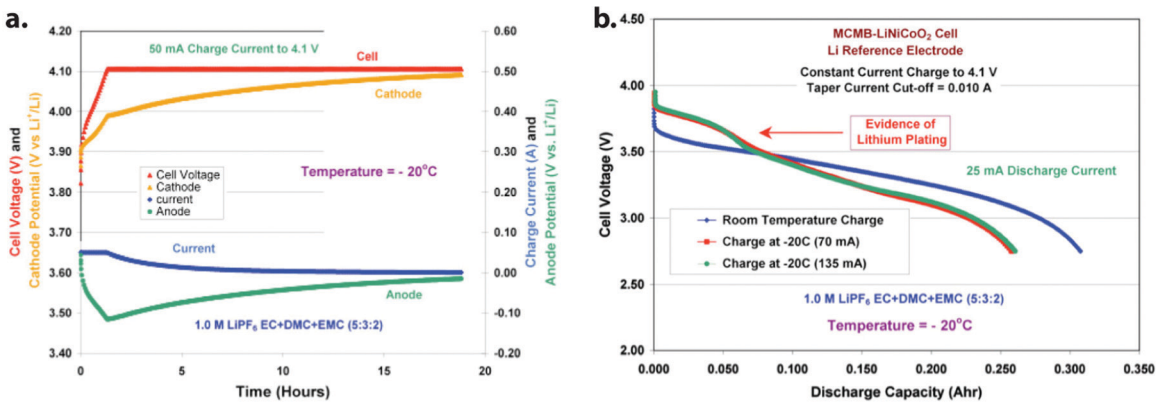

Fig. 7 (a) Electrode/cell voltage profiles during −20 °C charge of a MCMB‖$LiNi_{0.8}Co_{0.2}O_2$ cell with a Li reference electrode. Note that the anode potential drops below 0 V *vs.* Li/Li^+ almost immediately and remains there throughout charging, making Li plating possible. (b) Voltage–capacity plot of MCMB‖$LiNi_{0.8}Co_{0.2}O_2$ cells during −20 °C discharge following various charge protocols. A characteristic upper voltage plateau is present in the cells charged at −20 °C, indicating that lithium plating has occurred. Their discharge capacity is also reduced in comparison to the room-temperature-charged cell. Reprinted from ref. 48, copyright The Electrochemical Society. Reproduced by permission of IOP Publishing Ltd. All rights reserved.

mass transport and kinetic limitations. Solid-state transport limitations (*vide infra*) will increase at a high graphite SOC; as the graphite fills with Li, it becomes more difficult to insert additional Li atoms. The large concentration gradients that form at high charging rates, *i.e.* polarization overpotentials, also contribute to this drop.[23,45] Kinetic overpotentials are additionally impacted by such concentration gradients, as charge transfer resistance is dependent on the surface concentration of Li^+. Mass transport and kinetic overpotentials will also both increase with decreasing temperature, generally following Arrhenius-type dependencies. Waldmann *et al.* used a 3-electrode cell to demonstrate this temperature-dependent decrease in the anode potential;[46] during low-temperature charging, these overpotentials led to large amounts of Li plating at relatively low charging rates. A fraction of such Li metal deposits cannot be reversibly stripped, instead forming "dead" lithium which includes electronically-isolated metallic Li and graphite, as well as degradation products from the reaction of electrolyte with metallic Li. The formation of dead Li necessarily means a reduction in cyclable Li capacity; this has been quantified as a function of rate and cycle life at room temperature using destructive mass spectrometry titration.[47]

While the majority of literature has focused on fast charging at ambient temperatures (>20 °C), there have still been numerous studies characterizing Li plating on graphite during low-temperature operation. Electrochemical methods have been used to detect when Li plating has occurred at low temperature, including observation of a stripping plateau during discharge of spiral-rolled, 3-electrode LIBs (300–400 mA h, Gr‖NCO‖Li Ref.) operated at −40 °C (Fig. 7b),[48] along with d*V*/d*Q* analysis of discharge curves for LIBs (2.5 A h, 26 650 cylindrical Gr‖LFP) cycled at temperatures down to −30 °C.[14,49] The latter technique relies on the presence of the stripping plateau seen in the former. These d*V*/d*Q* studies also reveal an impedance rise after low-temperature charging, which the authors attributed to SEI growth from Li metal reacting with the electrolyte. This reaction of plated Li with the electrolyte is also noted by Ng *et al.* as the primary culprit for significant gas formation in their LIBs (50 A h, Gr‖NMC_{532} prismatic) cycled at −29 °C. This gas formation was shown to cause detrimental additional stresses on the electrodes, leading to eventual cell failure.[50]

Still, simple optical inspection of the graphite electrode remains the most common technique for Li plating detection upon post-mortem analysis. This necessarily requires enough Li to have plated for visual inspection to be possible. However, certain groups have expanded upon this relatively simple analysis to allow for more robust diagnoses; one of the previously-mentioned studies using d*V*/d*Q* and impedance spectroscopy also analyzed the deposited Li layer thickness to quantify the amount of Li plated.[14] Unfortunately, this still requires significant Li plating to have already occurred. Waldmann *et al.* have utilized optical inspection, combined with capacity fade monitoring, to label Li plating as the primary capacity fade mechanism for LIBs (1.5 A h, 18 650 cylindrical Gr‖NMC_{111} + LMO) cycled at temperatures down to −20 °C, relative to cells cycled up to 70 °C.[51] Ghanbari *et al.* used a more specialized technique—glow discharge optical emission spectroscopy—to characterize Li plating in cells, which showed homogeneous Li plating in cells cycled at −20 °C (2.5 A h, 26 650-format Gr‖LFP) relative to the "island" deposits formed in cells cycled at 45 °C (16 A h, Gr‖NMC).[52] It should be pointed out, though, that some of the differences in plating morphology could be attributed to different cell geometries. This optical emission technique can also discriminate between aging related to SEI growth *vs.* that related to Li plating. Each of these studies seems to suggest that Li plating is especially prevalent at low temperatures, and that it is the primary culprit for capacity fade of LIBs repeatedly charged under such conditions.

As others have noted, though, no technique to-date has been able to reliably detect the onset of Li plating in LIBs with high general sensitivity. d*V*/d*Q* analysis relies on the presence of a stripping plateau which is not always present, even when

lithium has 00]$262#[?down]?>plated,[53] and requires a slow discharge immediately after charging. Incidentally, a concise summary of all differential voltage analysis work performed for low temperature LIB applications thus far may be found in ref. 47 above. Optical inspection – perhaps the most universally-used technique – necessarily requires a large amount of Li deposition to have occurred; therefore, the damage of substantial, irreversible capacity loss must already be done. Differential open-circuit voltage analysis has recently shown some promise as a more general method for plating detection,[54] but requires further validation. Li plating detection techniques and their limitations, as well as ideas for Li plating mitigation, are more-thoroughly discussed in the previously mentioned fast charging and Li plating review articles. However, it should be emphasized that this current limitation in the field will need to be addressed in order to make low-temperature LIBs operation—where Li plating more readily occurs—a reality.

As a final comment, it should be noted that, under realistic operating conditions, *i.e.* large-format cells assembled in packs, the situation may be less bleak than it seems. Several authors have proposed tailoring battery pack design and/or charging protocols to take advantage of self-heating, so that overpotential is minimized by the end of charge and lithium plating is mitigated. Details are outside the scope of this review but may be readily found elsewhere.[55,56]

Non-electrolyte factors

There are, of course, physical processes relevant to low-temperature performance which are altogether divorced from electrolyte choice. While a detailed discussion falls outside the scope of this review, these factors may sometimes play a role in observed performance and, therefore, should be kept in mind. One such process is electron transport, which depends not only on bulk electrical conductivities (often quite low for cathode materials), but also on particle–particle interfacial contact. Luckily, modern electrode designs minimize these problems quite effectively, to the point where internal electrical resistance is generally negligible.[57]

Solid-state properties of the cathode and anode active materials also influence sub-zero behavior, most obviously through the dependence of surface area (and, thus, effective current density) on particle size. Indeed, an early study found that coke anode capacity at ≤ -20 °C was improved when average particle size was reduced from 25 μm to 6 μm.[58] More subtly, limited solid-state diffusion of lithium naturally causes the surface concentration of lithium to differ from the bulk when current is non-zero, which produces concentration polarization. The associated polarization resistance, although usually mild at room temperature and low rate, may become more significant with dropping temperature due to a decrease in lithium-ion solid-state diffusion coefficient.[59] A coupled electrochemical-thermal modeling study performed by Ji, Zhang and Wang has demonstrated that the limiting factors in large-format cells (2.2 A h 18 650 cylindrical) may be significantly different than in smaller cells due to non-isothermal conditions.[60] At −20 °C and low-rate discharge (0.001C), their model indeed predicted that interfacial kinetics dominate internal resistance; however, at higher rate (1C), self-heating effects reduced the influence of kinetic factors very early in the discharge process, whereas solid particle resistance at the anode grew continuously, becoming dominant towards the end of discharge. In all cases, accounting for self-heating resulted in higher capacity than predicted by an isothermal model. This result should caution the reader against generalizing any particular low-temperature result to batteries of dissimilar size or geometry.

Progress in low-temperature electrolyte design

When formulating a liquid electrolyte, there are three general components to adjust: additives, solvents and salts. The lines between these descriptors sometimes blur, as a particular chemical species may fall into multiple categories. For the sake of this review, we will consider a ''solvent'' to be a component with a melting point ≤ 40 °C that is present at >5 wt% concentration in the final mixture. Likewise, we will consider a ''primary salt'' to be a dissociable ionic substance containing Li^+, which is present at either >0.5 M or >5 wt% in the final mixture. Any reagent that falls outside these guidelines – for example, an ionic substance that is solid at room temperature and does not contain lithium, or a molecular liquid added to merely 2 wt% – would be considered an additive. These guidelines are largely arbitrary and chosen purely for convenience. Note that a single substance could be considered an additive in one study and a primary salt or solvent in another; the difference depends solely on the concentrations used. For the sake of relevance, we exclude $LiPF_6$ and EC/DEC/DMC/EMC from receiving focused discussion, since these materials are all well-studied and used commercially. More background on these standard electrolyte materials can be found in existing reviews.[13,61,62]

Additives

Electrolyte additives, by nature of their broad definition, take many forms and produce a variety of effects, such as reduced gas evolution or overcharge protection.[63] Most commonly, however, additives are intended to improve the cycling performance of LIBs, usually by stabilizing electrode interfaces to chemical or morphological changes over time. Given the strong correlation between electrode interfacial chemistry and low temperature performance, it is unsurprising that many additives have been investigated specifically for their effects below 0 °C. Additive formulations used by the references cited here may be found summarized in Table 1 along with their structures.

Fluoroethylene carbonate (FEC). Fluoroethylene carbonate (FEC) is one of the most popularly-studied additives for lithium-based batteries due to its favorable SEI-forming properties.[61,64,65] Naturally, given the critical role of interphase chemistry in LIB performance, FEC has found success in low-temperature electrolyte formulations. Liao *et al.* reported that adding 2 wt% FEC can modestly improve capacity, overpotential

Table 1 Additive summary table

Additive	Electrolyte	Ref.
FEC 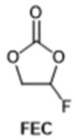 FEC	1 M $LiPF_6$, EC/PC/EMC (1 : 1 : 8 w/w) + 0.05 M $CsPF_6$ + various additives	38
	1 M $LiPF_6$, EC/PC/EMC (1 : 3 : 8 v/v) + 2 vol% FEC	66
	1 M $LiPF_6$, EC/PC/EMC (1 : 1 : 3 v/v) + 1 vol% FEC	67
	1 M $LiPF_6$, EC/PC/EMC (1 : 1 : 3 v/v) + 2 vol% FEC	
	1 M $LiPF_6$, EC/PC/EMC (1 : 1 : 3 v/v) + 5 vol% FEC	
	1 M $LiPF_6$, PC/DMC (1 : 1 v/v) + 5 vol% FEC	69
	1 M $LiPF_6$, PC/DMC (1 : 1 v/v) + 2 vol% CMDO + 5 vol% FEC	
	1 M $LiPF_6$, PC/DMC (1 : 1 v/v) + 3 vol% EC + 5 vol% FEC	
	1 M $LiPF_6$, PC/DMC (1 : 1 v/v) + 2 vol% CMDO + 3 vol% EC + 5 vol% FEC	
	1 M $LiPF_6$, EC/PC/EMC/DEC (20 : 5 : 55 : 20 v/v) + 2 wt% VC + 5 wt% FEC	86
	1 M $LiPF_6$, EC/PC/EMC (5 : 2 : 3 w/w) + 2 wt% FEC	87
TMSPi 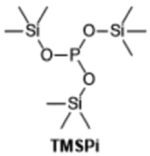 TMSPi	1 M $LiPF_6$, EC/PC/EMC (1 : 1 : 8 w/w) + 0.05 M $CsPF_6$ + various additives	38
	1 M $LiPF_6$, MA/EC/DEC/EMC (3 : 1 : 1 : 1 v/v) + 1 wt% TMSPi + 1 wt% PCS	74
Sulfur-based 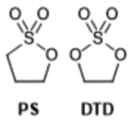 PS DTD	1 M $LiPF_6$, EC/PC/EMC (1 : 1 : 8 w/w) + 0.05 M $CsPF_6$ + various additives	38
	1 M $LiPF_6$, PC/DMC (1 : 1 v/v) + 2 vol% CMDO	69
	1 M $LiPF_6$, PC/DMC (1 : 1 v/v) + 2 vol% CMDO + 5 vol% FEC	
	1 M $LiPF_6$, PC/DMC (1 : 1 v/v) + 2 vol% CMDO + 3 vol% EC + 5 vol% FEC	
	1 M $LiPF_6$, MA/EC/DEC/EMC (3 : 1 : 1 : 1 v/v) + 1 wt% TMSPi + 1 wt% PCS	74
	1 M $LiPF_6$, EC/PC/EMC (1 : 1 : 3 w/w) + 1 wt% BuS	75
	1 M $LiPF_6$, EC/PC/EMC (1 : 1 : 3 v/v) + 1 vol% BuS	76
	1 M $LiPF_6$, EC/PC/EMC (1 : 1 : 3 v/v) + 2 vol% BuS	
	1 M $LiPF_6$, EC/PC/EMC (1 : 1 : 3 v/v) + 5 vol% BuS	
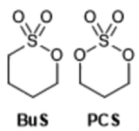 BuS PCS	0.9 M LiDFOB/$LiBF_4$ (5.4 : 1 w/w), EC/DMS/EMC (1 : 1 : 3 v/v)	77
	1 M $LiPF_6$, EC/EMC (1 : 2 w/w) + 0.5 wt% DMS	78
	1 M $LiPF_6$, EC/EMC (1 : 2 w/w) + 0.5 wt% DTD	
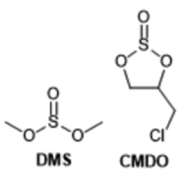 DMS CMDO	1 M $LiPF_6$, EC/DMC (1 : 1 v/v) + 1 wt% FI	80
	1 M $LiPF_6$, EC/DMC (1 : 1 v/v) + 2 wt% FI	
	1 M $LiPF_6$, EC/DMC (1 : 1 v/v) + 5 wt% FI	
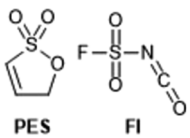 PES FI	1 M $LiPF_6$, EC/EMC (1 : 2 w/w) + 3 wt% PES	79

Table 1 (*continued*)

Additive	Electrolyte	Ref.
Li salts	1 M $LiPF_6$, EC/EMC/PC (4 : 7 : 1 w/w) + 1 wt% $LiPO_2F_2$	83
	1 M $LiPF_6$, EC/EMC (1 : 2 w/w) + 2 wt% $LiPO_2F_2$	84
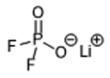	1 M $LiPF_6$, EC/EMC (1 : 2 w/w) + 0.25 wt% LiDFBOP	79
	1 M $LiPF_6$, EC/EMC (1 : 2 w/w) + 0.5 wt% LiDFBOP	
$LiPO_2F_2$	1 M $LiPF_6$, EC/EMC (1 : 2 w/w) + 1 wt% LiDFBOP	
	1 M $LiPF_6$, EC/PC/EMC/DEC (20 : 5 : 55 : 20 v/v) + 2.5 wt% Li202 + 2 wt% VC	85
	1 M $LiPF_6$, EC/PC/EMC/DEC (20 : 5 : 55 : 20 v/v) + 1 wt% Li202 + 2 wt% VC + 5 wt% FEC	86
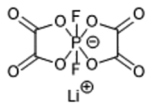	1 M $LiPF_6$, EC/PC/EMC/DEC (20 : 5 : 55 : 20 v/v) + 1 wt% PDMS-A + 2 wt% VC + 5 wt% FEC	
	1 M $LiPF_6$, EC/PC/EMC/DEC (20 : 5 : 55 : 20 v/v) + 1 wt% Li202 + 1 wt% PDMS-A + 2 wt% VC + 5 wt% FEC	
LiDFBOP	1 M $LiPF_6$, EC/EMC/MP (2 : 2 : 6 v/v) + 2 wt% [VC or PS]	104
	1 M $LiPF_6$, EC/EMC/MP (2 : 2 : 6 v/v) + 0.1 M [LiBOB, LiDFOB, or LiFSI]	
	0.45 M LiTFSI, EMIMFSI + 0.01 M LiBOB	116
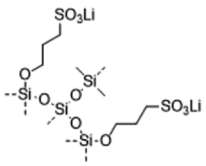		
Li202		
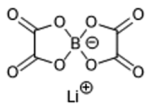		
LiBOB		
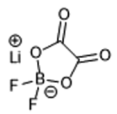		
LiDFOB		
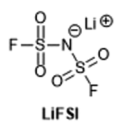		
LiFSI		
Other salts	1 M $LiPF_6$, EC/PC/EMC (x : 1 : 9-x w/w) + 0.05 M $CsPF_6$	15
	1 M $LiPF_6$, EC/PC/EMC (x : 2 : 8-x w/w) + 0.05 M $CsPF_6$	
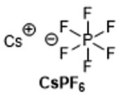	1 M $LiPF_6$, EC/PC/EMC (1 : 1 : 8 w/w) + 0.05 M $CsPF_6$ + various additives	38
	1 M $LiPF_6$, EC/PC/EMC (5 : 2 : 3 w/w) + 0.05 M $CsPF_6$	87
	1 M $LiPF_6$, EC/PC/EMC (3 : x : 7-x w/w) + 0.05 M $CsPF_6$	88
	1 M $LiPF_6$, EC/PC/EMC (x : 1 : 9-x w/w) + 0.05 M $CsPF_6$	89
$CsPF_6$	1 M $LiPF_6$, EC/PC/EMC (x : 2 : 8-x w/w) + 0.05 M $CsPF_6$	

and Coulombic efficiency on mesocarbon microbead (MCMB) graphite anodes at temperatures from −40 to 20 °C.[66] Combined electrochemical impedance spectroscopy (EIS) and X-ray photoelectron spectroscopy (XPS) results led the authors to conclude that the improvement resulted from a smoother, more conductive interphase formed by the additive, with the difference becoming more significant as temperature decreased. However, the authors' own data seems to indicate reduced charge transfer resistance in the presence of FEC as well, although they were unable to obtain accurate numbers for this component. Interestingly, the same group also showed a beneficial effect of FEC on a $LiFePO_4$ cathode,[67] although it should be mentioned that both studies presented data for only half cells with Li metal, for which FEC also produces notable effects.[68]

More commonly, FEC and other carbonates are used as individual components of a multi-additive mixture. For instance, Liu and coworkers demonstrated a complex, multi-additive system in which 0.5 wt% FEC played a crucial role to stabilize Gr‖NMC_{111} pouch cells at both −40 °C and 60 °C.[38] Another recent report by Wotango *et al.* demonstrated additive mixtures that included up to 5 wt% FEC.[69] Often, this additive is used in large enough concentration to qualify as a "solvent" component; such instances are discussed in the relevant section below.

Tris(trimethylsilyl)phosphite. Organophosphites have been proposed as LIB electrolyte additives for a variety of purposes, including flammability reduction[70] and high-voltage stability improvement.[71] In particular, tris(trimethylsilyl)phosphite *a.k.a.* TMSP or TMSPi has enjoyed recent popularity due to its passivating effect on metal oxides, resulting from the formation of a stable cathode electrolyte interphase (CEI) layer.[72] TMSPi has also been shown to participate in SEI formation on graphite

due to its reactivity with lithium alkoxides formed during EC degradation.[73] Given its influence at both sides of the cell, this molecule has received some recent study in low-temperature systems. A 2019 report by Liu *et al.* found TMSPi to be one of the most effective additives out of several at reducing Gr‖NCA full cell overpotential at −40 °C, thereby increasing capacity.[38] Interestingly, only 0.5 wt% was required for such improvement, while 1 wt% had a detrimental effect. Another paper from the same year demonstrated an electrolyte design including TMSPi which allowed a 5 V-class MCMB‖$LiNi_{0.5}Mn_{1.5}O_4$ (*a.k.a.* LNMO) cell to operate at temperatures down to −60 °C, including repeated charge/discharge at −5 °C at 0.3C rate without capacity fade (Fig. 8a and b).[74] Besides the expected cathode passivation, this additive was shown to significantly stabilize the anode SEI as well, preventing lithium metal deposition and reducing microscopic crack formation (Fig. 8c). These promising early results merit additional investigation, especially to untangle the relative contributions of TMSPi-formed CEI and SEI to the observed improvement at low temperatures.

Sulfur-containing molecules. Organosulfur compounds of varying structure and oxidation state have been heavily investigated as interphase-altering LIB electrolyte additives, including for low temperature cells. Butyl sultone (BuS) was reported for this purpose as early as 2006,[75] with the authors observing significant improvement in Gr‖$LiCoO_2$ full cell capacity and overpotential at temperatures from −20–70 °C. Detailed EIS study of a graphite anode revealed a notable drop in R_{ct} when 1 wt% BuS was present. A more current study found that BuS also has a positive effect on $LiFePO_4$ cathode capacity at low temperature, with up to 35% higher capacity (64.8 mA h g^{-1}) being available at 1C rate and −20 °C.[76] Additive amounts greater than 1%, however, proved detrimental. Dimethyl sulfite (DMS), a close chemical relative of DMC, has also been investigated by multiple groups.[77,78] Guo *et al.* very recently found that this additive is more effective than the commercially-popular 1,3,2-dioxathiolane-2,2-dioxide (DTD) at reducing capacity fade in Gr‖NMC_{523} pouch cells at −10 °C.[78] Li‖Gr half-cell studies indicated that both additives produced similar benefits in R_{SEI} and R_{ct} at room temperature, but that R_{SEI} was significantly lower for the DMS additive as temperature decreased. TEM imaging confirmed that the interphase formed by DMS was thinner and more uniform than that formed by DTD or in baseline electrolyte. Other compounds which have received focused study at subzero temperatures include

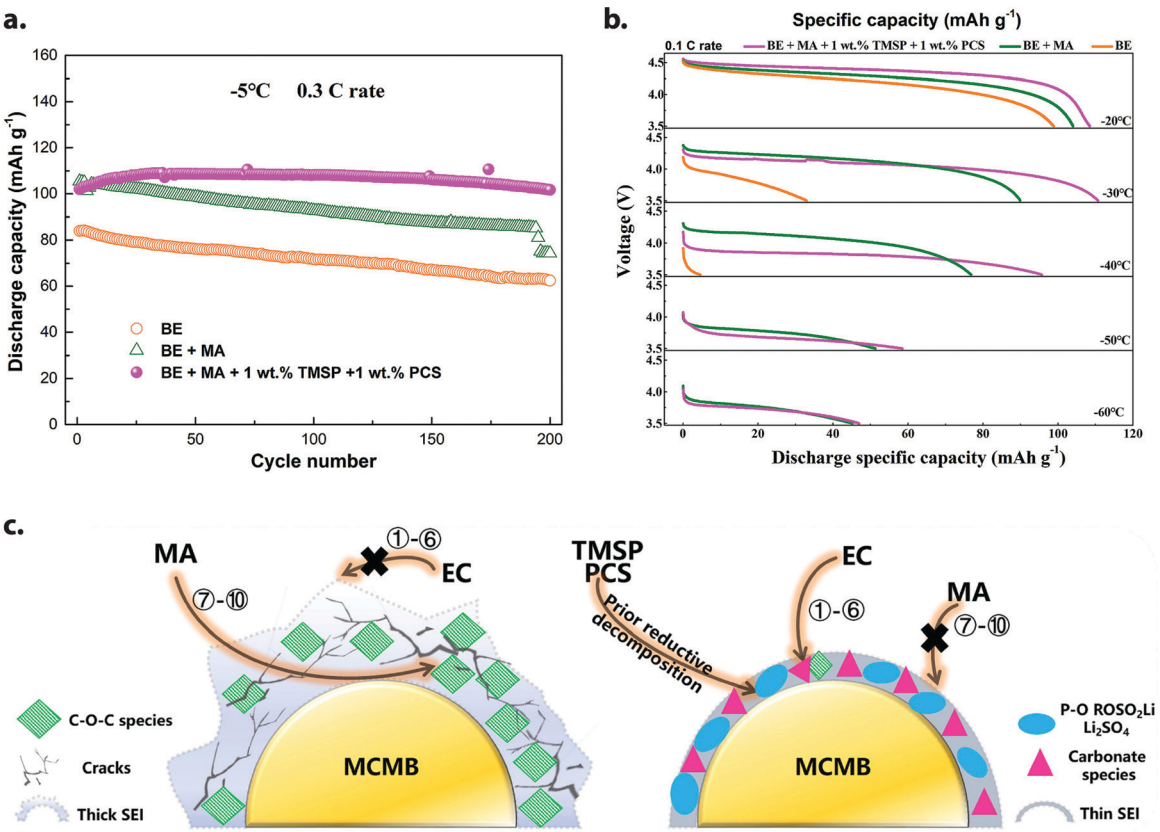

Fig. 8 (a) Cycling performance of MCMB‖$LiNi_{0.5}Mn_{1.5}O_4$ full cells (3.5–4.9 V) at −5 °C and 0.3C rate in commercially-available baseline electrolyte (BE), a modified electrolyte containing methyl acetate (BE + MA) and the preceding electrolyte with tris(trimethylsilyl)phosphite and 1,3-propanediol cyclic sulfate additives (BE + MA + 1 wt% TMSP + 1 wt% PCS). (b) Discharge characteristics of the above cell designs at −20 to −60 °C, following a 0.5C charge at room temperature. (c) Proposed working mechanism of the aforementioned phosphite and sulfate additives in this system, based on XPS analysis of cycled MCMB anodes. Formation of a thin, robust SEI prevents continuous decomposition of methyl acetate and resists Li dendrite growth during low-temperature charge. Reprinted/adapted from ref. 74 with permission from Elsevier.

1,3-propane sultone,[38] prop-1-ene-1,3-sultone[79] and 1,3-propanediol cyclic sulfate (see Fig. 7).[74]

More unique functionalities have also proven useful. Shi and coworkers recently demonstrated fluorosulfonyl isocyanate as a novel sacrificial additive which preferentially reduces to form a low-impedance SEI on graphite.[80] The resulting electrodes showed dramatically-improved rate performance in half cells with lithium, especially at low temperatures. Wotango *et al.* devised a novel chemical derivative of ethylene sulfite: 4-chloromethyl-1,3,2-dioxathiolane-2-oxide, which was used as a one of several additives to significantly improve Li‖MCMB half-cell performance at −10 °C.[69]

Lithium salts. Although many diverse lithium salts have been proposed as LIB additives, surprisingly few of these have been studied for their effect at low temperature specifically. One such salt is lithium difluorophosphate ($LiPO_2F_2$), which has been reported elsewhere to modify both cathode[81] and anode[82] interfacial chemistry. Yang *et al.* found that merely 1 wt% $LiPO_2F_2$ added to an electrolyte of 1 M $LiPF_6$ in EC/EMC/PC 4 : 7 : 1 w/w improved the relative capacity retention of Gr‖NMC_{523} cells at −30 °C from 9.6% to 57.9% (Fig. 9).[83] Galvanostatic cycling performance was also impacted: cells with control electrolyte experienced rapid capacity fading during repeated 0.5C charge/discharge at −20 °C, while additive-containing cells retained 91% of their initial capacity over 100 such cycles. Most recently, some of the same authors reported 2 wt% $LiPO_2F_2$ to improve the temperature range of 4.4 V pouch cells containing an electrolyte of 1 M $LiPF_6$ in EC/EMC 1 : 2 w/w.[84] Combined analytical results from both studies indicate that this additive acts as an interface-former on both graphite and NMC surfaces, with the resulting SEI and CEI exhibiting vastly-reduced resistance. Further study may be required to probe the mechanistic underpinnings of this effect. A structurally-related salt, lithium difluorobis(oxolato)phosphate (LiDFBOP), has also been shown to dictate anode and cathode interfacial makeup when added at 1%, with associated full-cell performance improvement at 0 °C.[79]

A particularly unique design comes from Ko *et al.*, who reported on a lithium-modified silica nanosalt ("Li202") synthesized by treating hydrophobic silica with LiH, followed by 1,3-propane sultone.[85] The resulting sulfonate-rich surface allowed the silica to form a stable dispersion (2.5 wt%) with an electrolyte solution of 1 M $LiPF_6$ in EC/PC/EMC/DEC 20 : 5 : 55 : 20 v/v + 2 wt% vinylene carbonate (VC). The presence of Li202 additive slightly improved the cycling performance of Gr‖$LiCoO_2$ coin cells at −20 °C when compared to the electrolyte alone and a non-functionalized silica dispersion. EIS analysis determined this effect to come from reduced R_{SEI} in the presence of the additive, a hypothesis which was corroborated by SEM images showing thinner interfacial layers. Several of the same authors also published a follow-up report showing a synergistic effect of Li202 additive with an acrylate-grafted PDMS additive.[86] Altogether, graphite‖$LiCoO_2$ cells with this dual-additive formulation showed improved capacity of up to 110 mA h g^{-1} at −20 °C and 0.1C discharge rate, as compared to 95 mA h g^{-1} without the additives. The combination appeared to significantly reduce both interfacial resistance and bulk electrolyte resistance as measured by EIS, although the exact reason was not explored.

Non-lithium salts. One of the most intriguing additives recently reported to improve low-temperature performance is $CsPF_6$, which has been systematically studied by Xu *et al.* (Fig. 10).[15,38,87–89] The effect of Cs^+ is reportedly due to its role in directing SEI formation: the cesium ion can accommodate only 1–2 EC molecules in its solvation shell and the reduction potential of $[Cs(EC)_{1-2}]^+$ solvates is higher than that of the $[Li(EC)_{3-4}]^+$ solvates also present. This results in an SEI dominated by the (desirable) decomposition products of EC,[87] even in electrolytes with competing solvents[88] and/or low EC content.[89] After optimization of both solvent and additive composition, 0.05 M $CsPF_6$ allowed Liu *et al.* to demonstrate 1 A h pouch cells (Gr‖NMC_{111}), which retained 0.69 A h discharge capacity at −18 °C and an impressive 0.37 A h discharge capacity at −40 °C, both at 1C rate. This was achieved without sacrificing room temperature or high temperature characteristics, either, as the same cells were able to cycle 1000 times with >85% capacity retention at 25 °C, and Gr‖NCA coin cells with the same electrolyte showed >60% retention after 300 cycles at 60 °C.

Solvents

With few exceptions, solvents make up the largest portion of any electrolyte, whether by weight, volume or mole fraction.

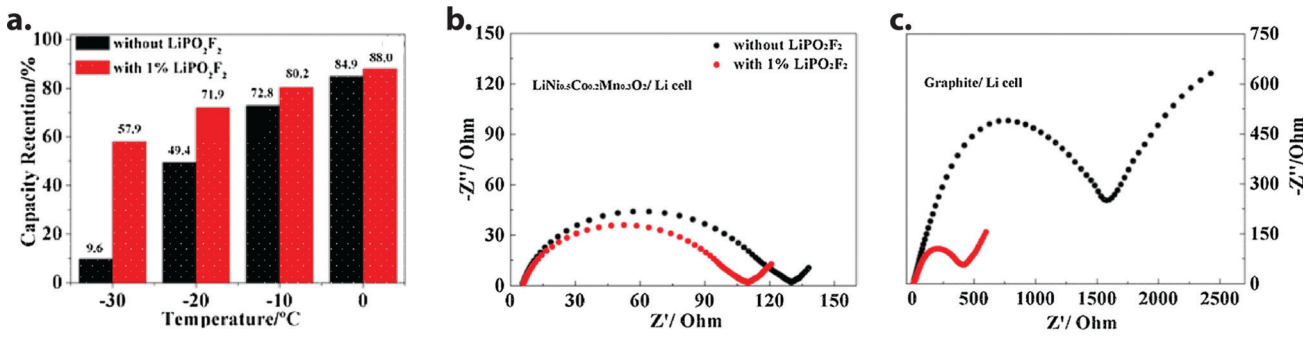

Fig. 9 (a) Discharge capacity retention of Gr‖NMC_{523} cells at sub-zero temperatures, relative to room temperature. Addition of 1 wt% $LiPO_2F_2$ to the standard electrolyte (1 M $LiPF_6$ in EC/EMC/PC 4 : 7 : 1 w/w) caused significant performance improvement. (b and c) Impedance response of fully-charged cathode and anode half-cells at 0 °C. The additive was found to reduce graphite interfacial resistance more than three-fold, while a comparatively minor improvement was observed for NMC_{532}. Reprinted/adapted from ref. 83 with permission from Elsevier.

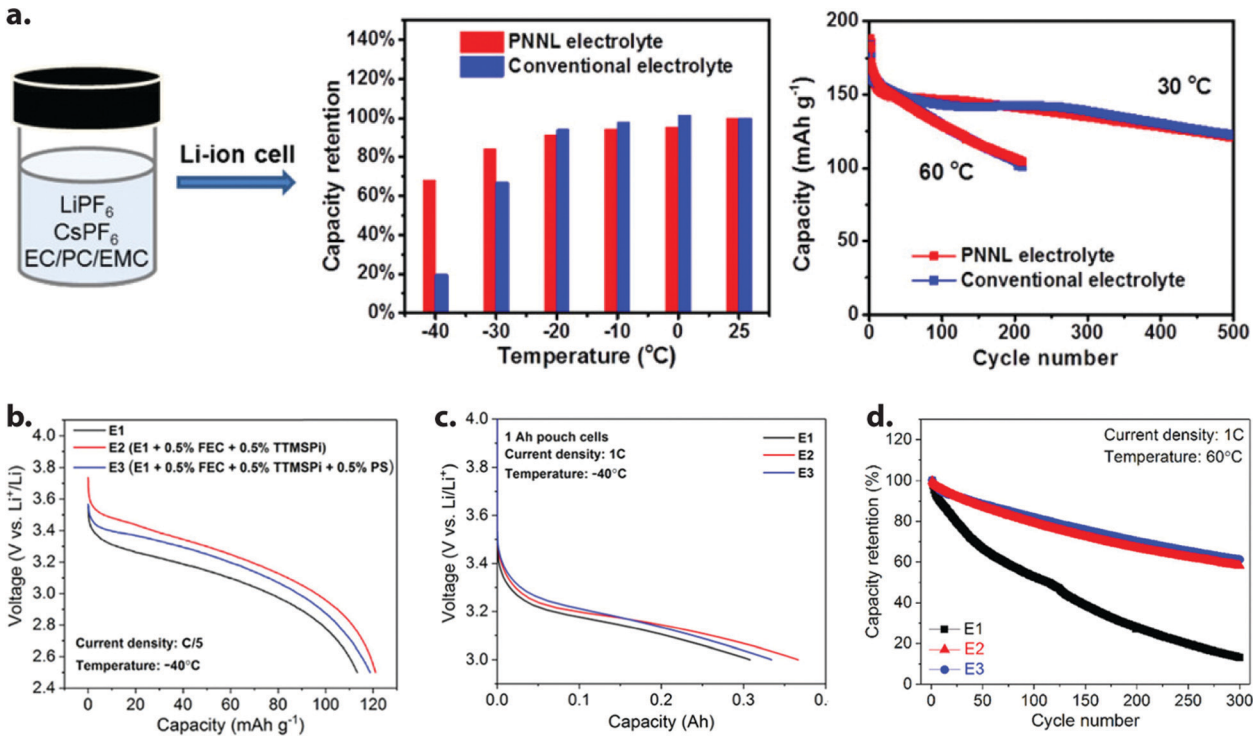

Fig. 10 (a) Comparison of electrolyte effect on Li-ion full cell performance at sub-zero temperatures (Gr‖NMC_{111} pouch cells) and room/elevated temperatures (Gr‖NCA coin cells). A small amount (0.05 M) of $CsPF_6$ additive enabled stable cycling in a lean-EC environment (1 M $LiPF_6$ in EC/PC/EMC 1 : 1 : 8 w/w) and vastly improved low-temperature capacity compared to a conventional formulation (1 M $LiPF_6$ in EC/EMC 3 : 7 v/v). Reprinted/adapted with permission from ref. 89. Copyright 2017 American Chemical Society. (b) Discharge voltage profiles of Gr‖NCA coin cells at −40 °C and C/5 rate in three electrolytes containing $CsPF_6$ additive, where E1 = 1 M $LiPF_6$ in EC/PC/EMC 1 : 1 : 8 w/w + 0.05 M $CsPF_6$. (c) 1C discharge of 1 A h-nominal Gr‖NMC_{111} pouch cells containing E1, E2, or E3 electrolyte at −40 °C. The electrolyte E2, containing 0.5 wt% each of FEC and TMSPi but no 1,3-propane sultone (PS), produced the best capacity (0.37 A h) under these harsh conditions. (d) Capacity retention of Gr‖NCA coin cells containing E1, E2, or E3 during 1C galvanostatic cycling at 60 °C. The presence of 0.5 wt% PS in electrolyte E3 gives a slight advantage at elevated temperature. Reprinted/adapted with permission from ref. 38. Copyright 2019 American Chemical Society.

Their principal job is to dissolve and dissociate the primary salt into free ions, which carry the internal current of the battery. This process is facilitated by solvents with high dielectric permittivity and electron donor number, such as EC, which forms strong solvation complexes with Li^+. Unfortunately, this presents a dilemma at low temperatures, where desolvation becomes the rate-limiting step in charge transfer (*vide supra*). This has driven a large body of research into alternative solvents which can replace or augment EC without sacrificing the favorable ion transport properties it endows. Such efforts are additionally complicated by the secondary role of LIB electrolyte solvents: interfacial compatibility. Solvent blends must be stable to oxidation at high cathode potentials (>4 V) and form sufficiently inert SEI layers at graphite anodes, as discussed previously. Therefore, alternative solvents are often used in combination with passivating additives in order to realize the benefits of low-EC-content electrolytes at sub-zero temperature without sacrificing cycle life. Solvent formulations investigated by the references cited here are summarized in Table 2 along with their structures.

Propylene carbonate. Propylene carbonate (PC) is a well-known polar aprotic solvent (ε = 65)[16] with a wide liquid range (−49 to 242 °C),[90] properties which have garnered attention since the early days of LIB development. While the idea of a PC-based electrolyte was initially shelved due to its tendency to co-intercalate into graphite, modern developments in additive and solvent formulation have enabled its reintroduction with the suppression of harmful side effects. Because the melting point and viscosity of PC compare favorably to EC,[17] replacing some or all of the latter can naturally improve conductivity at low temperature and dramatically reduce crystallization tendency, a factor that has been exploited by many researchers in this area. In fact, many of the studies summarized in this review use baseline electrolytes containing some quantity of PC.

For instance, as mentioned previously, Xu and coworkers have published a series of reports on $CsPF_6$ additive, the original purpose of which was to stabilize graphite anodes in a majority-PC electrolyte.[15,38,87–89] In one study from 2017, Li *et al.* thoroughly compared the thermal properties and ionic conductivity of electrolytes containing varying ratios of EC, PC and EMC with constant salt concentrations (1.0 M $LiPF_6$ and 0.05 M $CsPF_6$).[89] Addition of PC was found to significantly reduce both thermodynamic liquidus temperature and the kinetic precipitation point, with a 1 : 1 : 8 blend exhibiting values of −58.4 °C and −67.2 °C, respectively (Fig. 11a). Moreover, conductivity uniformly increased with decreasing EC content at temperatures below −20 °C, with

Table 2 Solvent summary table

Solvent	Electrolyte	Ref.
PC 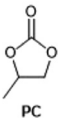	1 M $LiPF_6$, EC/PC/EMC (x:1:9-x w/w) + 0.05 M $CsPF_6$	15
	1 M $LiPF_6$, EC/PC/EMC (x:2:8-x w/w) + 0.05 M $CsPF_6$	
	1 M $LiPF_6$, EC/PC/EMC (1:1:8 w/w) + 0.05 M $CsPF_6$ + various additives	38
	1 M $LiPF_6$, EC/PC/EMC (1:3:8 v/v) + 2 vol% FEC	66
	1 M $LiPF_6$, EC/PC/EMC (1:1:3 v/v) + 1 vol% FEC	67
	1 M $LiPF_6$, EC/PC/EMC (1:1:3 v/v) + 2 vol% FEC	
	1 M $LiPF_6$, EC/PC/EMC (1:1:3 v/v) + 5 vol% FEC	
	1 M $LiPF_6$, PC/DMC (1:1 v/v) + 5 vol% FEC	69
	1 M $LiPF_6$, PC/DMC (1:1 v/v) + 2 vol% CMDO + 5 vol% FEC	
	1 M $LiPF_6$, PC/DMC (1:1 v/v) + 3 vol% EC + 5 vol% FEC	
	1 M $LiPF_6$, PC/DMC (1:1 v/v) + 2 vol% CMDO + 3 vol% EC + 5 vol% FEC	
	1 M $LiPF_6$, EC/PC/EMC (1:1:3 w/w) + 1 wt% BuS	75
	1 M $LiPF_6$, EC/PC/EMC (1:1:3 v/v) + 1 vol% BuS	76
	1 M $LiPF_6$, EC/PC/EMC (1:1:3 v/v) + 2 vol% BuS	
	1 M $LiPF_6$, EC/PC/EMC (1:1:3 v/v) + 5 vol% BuS	
	1 M $LiPF_6$, EC/EMC/PC (4:7:1 w/w) + 1 wt% $LiPO_2F_2$	82
	1 M $LiPF_6$, EC/PC/EMC/DEC (20:5:55:20 v/v) + 2.5 wt% Li202 + 2 wt% VC	85
	1 M $LiPF_6$, EC/PC/EMC/DEC (20:5:55:20 v/v) + 2 wt% VC + 5 wt% FEC	86
	1 M $LiPF_6$, EC/PC/EMC/DEC (20:5:55:20 v/v) + 1 wt% Li202 + 2 wt% VC + 5 wt% FEC	86
	1 M $LiPF_6$, EC/PC/EMC/DEC (20:5:55:20 v/v) + 1 wt% PDMS-A + 2 wt% VC + 5 wt% FEC	
	1 M $LiPF_6$, EC/PC/EMC/DEC (20:5:55:20 v/v) + 1 wt% Li202 + 1 wt% PDMS-A + 2 wt% VC + 5 wt% FEC	
	1 M $LiPF_6$, EC/PC/EMC (5:2:3 w/w) + 0.05 M $CsPF_6$	87
	1 M $LiPF_6$, EC/PC/EMC (3:x:7-x w/w) + 0.05 M $CsPF_6$	88
	1 M $LiPF_6$, EC/PC/EMC (x:1:9-x w/w) + 0.05 M $CsPF_6$	89
	1 M $LiPF_6$, EC/PC/EMC (x:2:8-x w/w) + 0.05 M $CsPF_6$	
	1 M $LiBF_4$, PC/EMC/MB/EC (19:19:57:5 w/w)	106
	1 M $LiPF_6$, THTO/PC (x:100-x mol/mol)	118
	1 M $LiBF_4$, PC/EC/EMC (1:1:3 w/w)	122
	1 M LiBOB, PC/EC/EMC (1:1:3 w/w)	125
	1 M LiDFOB, PC/EC/EMC (3:3:4 w/w)	128
FEC, VC, other carbonates 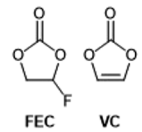 FEC VC 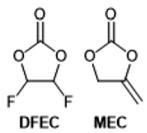 DFEC MEC 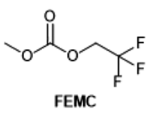 FEMC	1 M $LiPF_6$, EC/EMC (3:7 w/w) + 2 wt% VC	
	1 M $LiPF_6$, [EA or MP]/[VC or FEC] (99:1 w/w)	91
	1 M $LiPF_6$, [EA or MP]/[VC or FEC] (97:3 w/w)	
	1 M $LiPF_6$, [EA or MP]/[VC or FEC] (9:1 w/w)	
	1 M $LiPF_6$, EMC + 1% wt [VC, FEC, DFEC, or MEC]	92
	1 M $LiPF_6$, EMC + 2% wt [VC, FEC, DFEC, or MEC]	
	1 M $LiPF_6$, EMC + 3% wt [VC, FEC, DFEC, or MEC]	
	1 M $LiPF_6$, EMC + 4% wt [VC, FEC, DFEC, or MEC]	
	1 M $LiPF_6$, EMC + 5% wt [VC, FEC, DFEC, or MEC]	
	1 M $LiPF_6$, EC/DEC (1:1 v/v)	93
	1 M $LiPF_6$, EC/DEC (1:1 v/v) + 10% VC	
	1 M $LiPF_6$, EC/DEC (1:1 v/v) + 10% FEC	
	1 M $LiPF_6$, EC/DEC (1:1 v/v) + 10% DFEC	
	4.2 M LiFSI, FEC/FEMC (1:2 v/v)	94
	1.28 M LiFSI, FEC/FEMC/D2 (1:2:7 v/v)	
	0.7 M LiBETI, FEC/DEC/M3 (1:5:14 v/v)	
	1.2 M $LiPF_6$, EC/EMC (3:7 w/w) + 10 wt% FEC	95
	1 M $LiPF_6$, FEC/DMC (1:4 w/w)	139
	1 M $LiPF_6$, EC/DMC/DEC (1:3:1 v/v) + 60% EA + 10% FEC	140

Table 2 (*continued*)

Solvent	Electrolyte	Ref.
Linear esters (EA, MB, etc.)	1 M $LiPF_6$, MA/EC/DEC/EMC (3 : 1 : 1 : 1 v/v) + 1 wt% TMSPi + 1 wt% PCS	74
	1 M $LiPF_6$, [EA or MP]/[VC or FEC] (99 : 1 w/w)	91
	1 M $LiPF_6$, [EA or MP]/[VC or FEC] (97 : 3 w/w)	
	1 M $LiPF_6$, [EA or MP]/[VC or FEC] (9 : 1 w/w)	
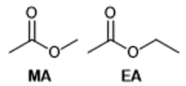 MA EA	1 M $LiPF_6$, EC/EMC/[MP, EP, MB, EB, PB, or BB] (2 : 6 : 2 v/v)	99
	1 M $LiPF_6$, EC/EMC/[TFEB, TFEA, ETFA, or MPFP] (2 : 6 : 2 v/v)	100
	1 M $LiPF_6$, EC/EMC/[TFEB, TFEA, ETFA, or MPFP] (2 : 4 : 4 v/v)	
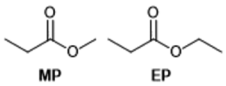 MP EP	1 M $LiPF_6$, EC/EMC/TFENH (6 : 24 : 3 v/v)	101
	1 M $LiPF_6$, EC/EMC/TFENH (6 : 24 : 6 v/v)	
	1 M $LiPF_6$, EC/EMC/TFENH (6 : 24 : 10 v/v)	
	1 M $LiPF_6$, EC/EMC/TFENH (6 : 24 : 30 v/v)	
	1 M $LiPF_6$, EC/EMC/TFENH (6 : 24 : 60 v/v)	
	1 M $LiPF_6$, TFENH	
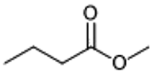 MB	1.2 M $LiPF_6$, EC/EMC/DMC/[MP, EA, or MB] (23.75 : 4.75 : 66.5 : 5 v/v) + 2 wt% VC	102
	1.2 M $LiPF_6$, EC/EMC/DMC/[MP, EA, or MB] (20 : 4 : 56 : 20 v/v) + 2 wt% VC	
	1.2 M $LiPF_6$, EC/EMC/DMC/[MP, EA, or MB] (15 : 3 : 42 : 40 v/v) + 2 wt% VC	
	1.2 M $LiPF_6$, EC/EMC/DMC/[MP, EA, or MB] (10 : 2 : 28 : 60 v/v) + 2 wt% VC	
	1.2 M $LiPF_6$, [EC/EMC/DMC (25 : 5 : 70 v/v)]/[MA or MP] (8 : 2 w/w) + 2 wt% [VC or FEC]	103
	1.2 M $LiPF_6$, [EC/EMC/DMC (25 : 5 : 70 v/v)]/[MA or MP] (6 : 4 w/w) + 2 wt% [VC or FEC]	
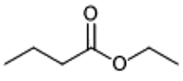 EB	1 M $LiPF_6$, EC/EMC/MP (2 : 2 : 6 v/v) + 2 wt% [VC or PS]	104
	1 M $LiPF_6$, EC/EMC/MP (2 : 2 : 6 v/v) + 0.1 M [LiBOB, LiDFOB, or LiFSI]	
	1.2 m $LiPF_6$, [EC/EMC/DMC (25 : 5 : 70 w/w)]/[MA, EA, MP, or MB] (4 : 1 w/w)	105
	1 M $LiBF_4$, PC/EMC/MB/EC (19 : 19 : 57 : 5 w/w)	106
	1 M $LiPF_6$, EC/EMC/EA (1 : 5 : 4 v/v)	
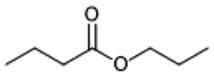 PB	2 M LiTFSI, EA	107
	1 M LiDFOB, GBL/MB (1 : 1 v/v)	109
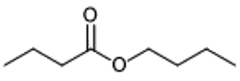 BB		
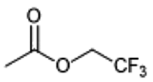 TFEA		
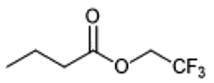 TFEB		
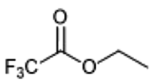 ETFA		
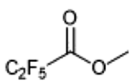 MPFP		
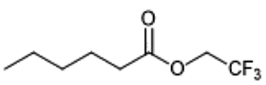 TFENH		
	1 M LiDFOB, GBL/MB (1 : 1 v/v)	109
Lactones	1 M LiBOB, GBL	110
	1 M LiBOB, GBL/DMC (7 : 3 w/w)	
	1 M LiBOB, GBL/F-EPE (7 : 3 w/w)	
 GBL	1 M LiDFOB, GBL/F-EPE (7 : 3 w/w)	111
	1 M $LiBF_4$, EC/DMC/GBL (1 : 1 : 1 w/w)	125
	See patent text	126
	0.1 m LiTFSI, $PP_{13}TFSI$	112

Table 2 (*continued*)

Solvent	Electrolyte	Ref.
RTILs	0.2 m LiTFSI, $PP_{13}TFSI$	
	0.3 m LiTFSI, $PP_{13}TFSI$	
	0.4 m LiTFSI, $PP_{13}TFSI$	
	0.4 m LiTFSI, $PP_{13}TFSI$/DEC (8 : 2 w/w)	
	0.4 m LiTFSI, $PP_{13}TFSI$/DEC (6 : 4 w/w)	
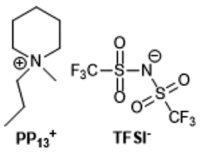	$Pyr_{14}TFSI$	114
	$Pyr_{13}FSI/Pyr_{14}TFSI$ (0.248 : 0.752 mol/mol)	
	$Pyr_{13}FSI/Pyr_{14}TFSI$ (0.568 : 0.432 mol/mol)	
	$Pyr_{13}FSI/Pyr_{14}TFSI$ (0.836 : 0.164 mol/mol)	
	$Pyr_{13}FSI$	
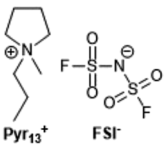	0.45 M LiTFSI, EMIMFSI	116
	0.45 M LiTFSI, EMIMFSI + 0.01 M LiBOB	
	1 M $LiPF_6$, EC/EMC (1 : 2 w/w) + 0.5 wt% $EMIMBF_4$	117
	1 M $LiPF_6$, EC/EMC (1 : 2 w/w) + 1 wt% $EMIMBF_4$	
	1 M $LiPF_6$, EC/EMC (1 : 2 w/w) + 2 wt% $EMIMBF_4$	
	1 M $LiPF_6$, EC/EMC (1 : 2 w/w) + 5 wt% $EMIMBF_4$	
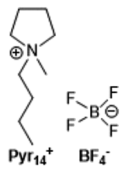		
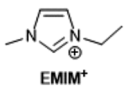		
Others	0.9 M LiDFOB/$LiBF_4$ (5.4 : 1 w/w), EC/DMS/EMC (1 : 1 : 3 v/v)	77
	1.28 M LiFSI, FEC/FEMC/D2 (1 : 2 : 7 v/v)	94
	0.7 M LiBETI, FEC/DEC/M3 (1 : 5 : 14 v/v)	
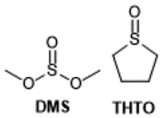	1 M LiBOB, GBL/F-EPE (7 : 3 w/w)	110
	1 M LiDFOB, GBL/F-EPE (7 : 3 w/w)	111
	1 M $LiPF_6$, THTO/PC (x : 100-x mol/mol)	118
	0.1 M LiTFSI, CH_3F/CO_2 (19 : 1 w/w)	119
	0.2 M LiTFSI, CH_3F/CO_2 (19 : 1 w/w)	
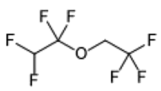	0.3 M LiTFSI, 0.3 M THF, CH_3F/CO_2 (19 : 1 w/w)	120
	1.2 M LiTFSI, 1 M AN, CH_3F/CO_2 (19 : 1 w/w)	121
	21 m LiTFSI, H_2O	131
	21 m LiTFSI, H_2O + 9.25 m LiTFSI, DMC	
	15.3 m LiTFSI, H_2O/AN (1 : 1 mol/mol)	
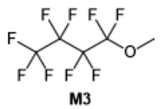	Composition series, see text	132
	5.2 m LiTFSI, H_2O	133
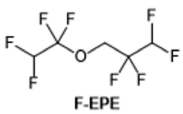		
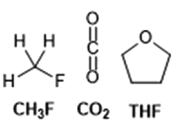		
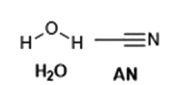		
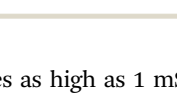		

values as high as 1 mS cm^{-1} at −40 °C being obtainable for the 1 : 1 : 8 blend (Fig. 11b). This relatively simple ternary mixture enabled both Gr‖NCA coin cells and Gr‖NMC_{111} pouch cells to discharge >65% of their normal capacity at −40 °C and C/5 discharge rate (Fig. 11c).

FEC, VC and other carbonates. Other carbonates have also been tested for their ability to fully replace EC, including VC[91] and FEC.[92–95] Dahn and coworkers have recently reported on electrolytes containing VC as the sole carbonate component, which allowed cells to retain 40% of their normal discharge energy at −14 °C and a blistering 4C rate, whereas a traditional EC/EMC electrolyte with 2 wt% VC could not discharge at all at rates above 2C at this temperature.[91] A later study from the same group found that a 5 : 95 FEC/EMC electrolyte produced

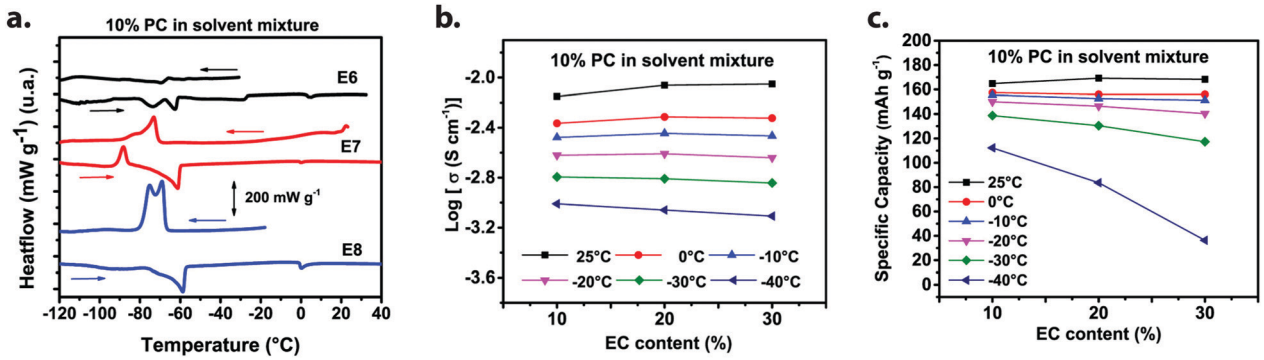

Fig. 11 (a) Differential scanning calorimetry results for electrolytes containing 10 wt% PC and either 30 wt% EC (E6), 20 wt% EC (E7), or 10 wt% EC (E8), with the balance being EMC. Reduction of EC content in the presence of PC allows the liquid range of the electrolyte to be extended below −50 °C. (b) Temperature-dependent conductivity of 10% PC electrolytes with varying EC content. Conductivity varies inversely with %EC below −20 °C, although the overall variation is small. (c) C/5 discharge capacity of Gr‖NCA coin cells at varying temperatures as a function of EC content. The 1 : 1 : 8 EC/PC : EMC blend performs best under sub-zero conditions. Reprinted/adapted with permission from ref. 89. Copyright 2017 American Chemical Society.

much lower R_{ct} in Gr‖NMC_{442} full cells compared to 5 : 95 VC/EMC.[92] While these later results were obtained at room temperature, they may have implications for low-temperature performance as well, given that R_{ct} increases in relative importance with decreasing temperature. A striking example of electrolyte design using FEC comes from Fan *et al.*, who recently published a report on electrolytes with high fluorine content utilizing FEC as the primary high-dielectric solvent

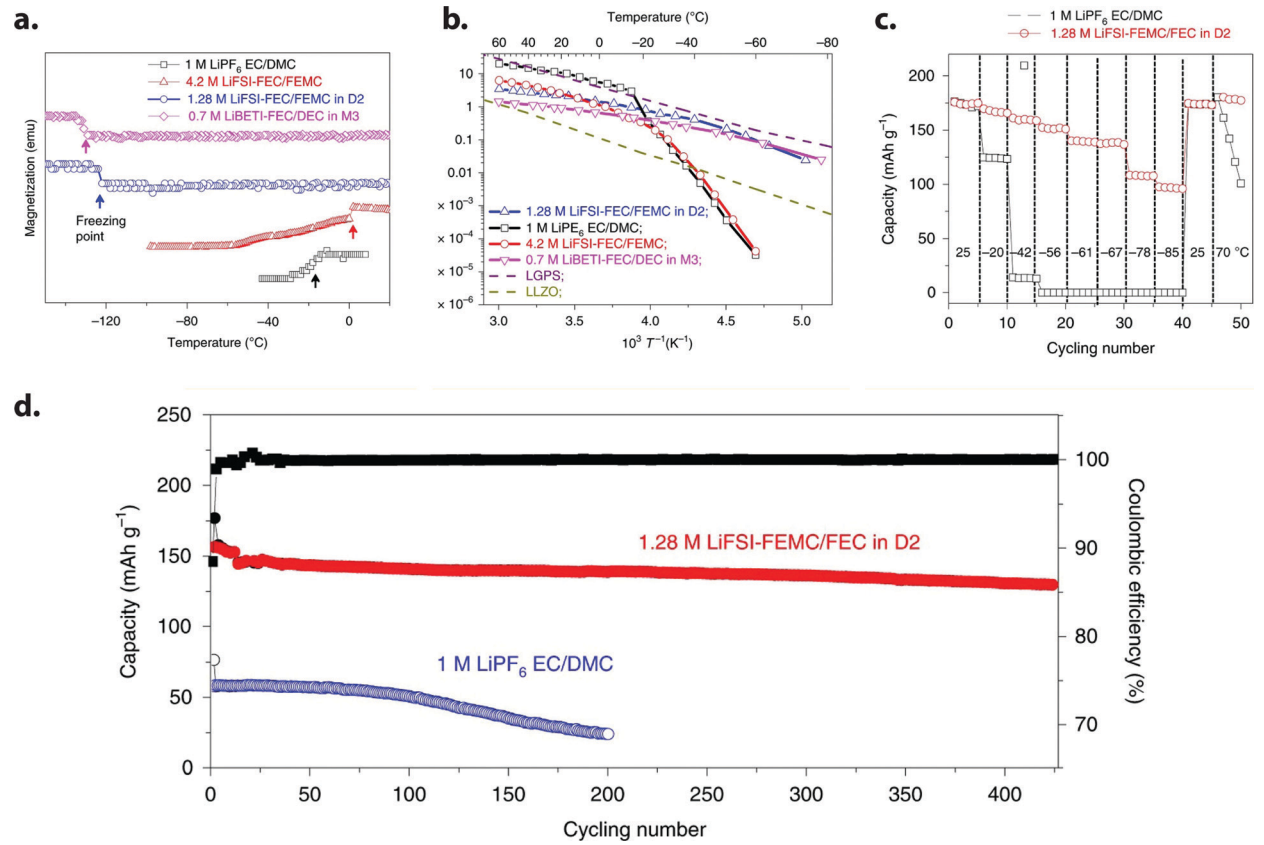

Fig. 12 (a) Freezing points of highly-fluorinated FEC-based electrolytes as measured by a superconducting quantum interference magnetometer device. (b) Temperature-dependent conductivity of several electrolytes, with two common solid electrolytes as references (dashed lines). The highly-fluorinated electrolytes diluted with inert solvents exhibit conductivities $>10^{-3}$ S cm^{-1} at room temperature and remain above 10^{-5} S cm^{-1} down to −80 °C. (c) Variable-temperature C/15 cycling of Li‖NCA half cells containing a highly-fluorinated electrolyte *vs.* a standard formulation. The fluorinated electrolyte enables cell function between −95 to 70 °C, whereas EC/DMC electrolyte produces negligible capacity below −20 °C and experiences rapid capacity fade at 70 °C. (d) C/3 cycling of Li‖NCA at −20 °C, which shows excellent discharge capacity and coulombic efficiency in the fluorinated electrolyte with minimal capacity fade. Reprinted by permission from Springer Nature: ref. 94, copyright 2019.

component.[94] These authors dissolved a high concentration of fluorinated salts LiFSI or LiBETI salts in 1 : 3 mixtures of FEC with methyl (2,2,2-trifluoroethyl) carbonate or DEC, respectively. The concentrated electrolytes were then further diluted into inert fluorinated solvents, which cannot ordinarily dissolve lithium salts, but are miscible with the pre-solvated blends. The resulting localized high-concentration electrolytes remained liquid below −120 °C (Fig. 12a), an astonishing low-temperature limit for any organic fluid. Their conductivities also showed unexpectedly weak thermal dependence, varying merely two orders of magnitude (10^{-5}–10^{-3} S cm^{-1}) from −80 °C to 25 °C (Fig. 12b). Moreover, due to the high ratio of salt to (coordinating) solvent molecules, the average solvation energy of Li^+ – and thus, indirectly, the charge transfer resistance – was predicted to be significantly reduced (although it was not directly measured). Altogether, this combination of favorable electrolyte properties allowed the authors to successfully operate Li‖NCA cells from −95 to 70 °C (Fig. 12c and d). To our knowledge, this is the widest temperature range ever reported for a lithium-based battery with a liquid electrolyte. It is also notable that the authors reported Coulombic efficiencies >99% for a large number of anode materials (lithium metal, Gr, LTO) and cathode materials (NMC_{811}, NCA, LiNMO, $LiCoMnO_4$) with this electrolyte, demonstrating the universality of the design approach.

Esters/lactones. Besides carbonates, esters have received the most consideration as electrolyte solvents for low temperature LIBs, along with their cyclic variants known as lactones. This is largely due to the pioneering early work of M. C. Smart and coworkers,[96,97] who investigated many of these molecules as solvent components to supplement the traditional EC, DEC, *etc.* In particular, linear aliphatic esters (or simply ''esters'') possess a winning combination of low viscosity, low melting point and moderate polarity – all characteristics that encourage fast Li^+ transport over a wide temperature range. Nonetheless, they have several critical drawbacks, including high volatility (*i.e.* flammability) and reduced electrochemical window compared to carbonates. The simplest esters, such as methyl formate[98] and ethyl acetate,[96] are cathodically unstable to lithiated graphite and do not produce an effective passivating layer upon their breakdown. Although this may be remedied somewhat by inclusion of EC, R_{SEI} and R_{ct} become quite high in such electrolytes after extended cycling, rendering them useless in the long-term. However, slightly-larger esters like ethyl butyrate appear to be less reactive in this regard and can be successfully added to carbonate mixtures to improve low-temperature capacity without incurring large penalties elsewhere.[97] It should be noted that, according to the preceding reference, ester cosolvent addition reduces high-voltage stability as well, necessitating careful control over charge conditions.

Several design strategies have emerged to balance the advantages and drawbacks of ester (co-)solvents. Structure/blend optimization is perhaps the simplest solution, as demonstrated by the comprehensive screening published by Smart *et al.* in 2010.[99] Amongst the many formulations studied by these authors, methyl propionate (MP) was found to be most effective (Fig. 13a), as an electrolyte of 1 M $LiPF_6$ in EC/EMC/MP 2 : 6 : 2 v/v enabled nominal 7 A h Gr|$LiNi_{0.8}Co_{0.2}O_2$ cells to retain over 5 A h down to −60 °C. Another recurring concept involves partial fluorination, as in the case of 2,2,2-trifluoroethyl butyrate[100] and 2,2,2-trifluoroethyl *n*-caproate[101] among others, which generally tends to improve high-voltage stability and modify SEI composition. The most common recent development, however, has seen ester-based formulations paired with interface-modifying additives, including VC,[91,102–104] FEC[103,105] and others.[74,104] For instance, Jones *et al.* tested a series of additives for their ability to inhibit lithium plating during low-temperature charge in a MP-rich electrolyte, finding 0.1 M LiFSI to be most effective.[104] In at least one case, additives have made it possible to eliminate EC from the electrolyte entirely, with a MP : VC 95 : 5 w/w electrolyte allowing acceptable capacity retention during 40 °C cycling of Gr‖NMC_{111} pouch cells and enabling significantly-improved rate performance at −14 °C compared to an EC/EMC/VC mixture.[91] Inclusion of such additives also frees up the design space to include more-reactive, but less-viscous and higher-polarity esters like methyl acetate.[103] Shorter esters have also proven valuable to the performance of

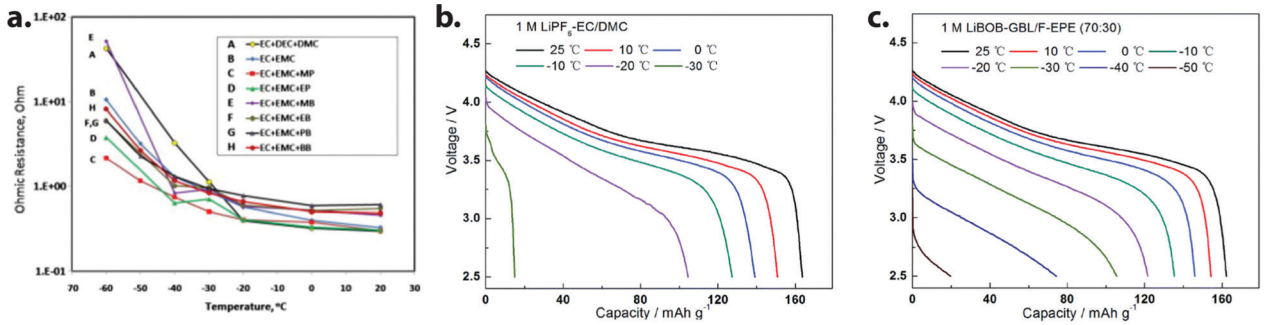

Fig. 13 (a) Temperature-dependent series resistance of MCMB‖$Li_xNi_yCo_{1-y}O_2$ pouch cells containing electrolytes of 1 M $LiPF_6$ in EC (20 vol%), EMC (60 vol%) and various esters (20 vol%). Methyl propionate (MP) produced the best results. Reprinted from ref. 99, copyright The Electrochemical Society. Reproduced by permission of IOP Publishing Ltd. All rights reserved. (b and c) 0.1C discharge of Gr‖NMC_{111} coin cells at various temperatures. The control electrolyte of 1 M $LiPF_6$ in EC/DMC 1 : 1 v/v caused rapid capacity loss below −20 °C, with the cell becoming inoperable at −30 °C. On the other hand, a carbonate-free electrolyte of 1 M LiBOB in 70 wt% gamma-butyrolactone (GBL) and 30 wt% hydrofluoroether (F-EPE) enabled the cell to retain nearly half its capacity down to −40 °C, while matching the performance of the control at 25 °C. Reproduced and adapted from ref. 110.

LIBs without graphite: Chen and coworkers tested LTO‖lithium manganese oxide cells with a variety of electrolytes and found an ethyl acetate-containing commercial blend to produce the lowest total impedance, with resulting cells able to pass the USABC cold cranking test at −30 °C.[106] Similarly, an all-organic battery design has been demonstrated at −70 °C using an electrolyte with ethyl acetate as the sole solvent component.[107]

We would be remiss to conclude our discussion of ester electrolytes without mentioning lactones. Unlike linear esters, which generally play a similar role to linear carbonates in electrolyte design, cyclic lactones are polar enough to replace EC/PC partially or entirely. The best-studied member of this class, gamma-butyrolactone (GBL), has a relative dielectric constant of 42 at room temperature[108] – around half that of EC, but still large enough to permit effective ionization of Li^+ salts. It also remains liquid over a wider range (−44 to 204 °C) and possesses lower viscosity (1.7 cP at 25 °C) than EC, both valuable qualities for a low-temperature electrolyte solvent. Like other esters, however, it is unable to form a passivating SEI on graphite,[13] a discovery that all-but-killed research into GBL electrolytes early in the development of LIBs. Yet recent progress may provide a way forward, as the responsibility for interfacial stability shifts away from solvents and towards salts/additives. For instance, Lazar and Lucht reported successful cycling of Gr‖NCA coin cells in an all-ester electrolyte of GBL and methyl butyrate (1 : 1 vol) containing 1 M lithium difluoro(oxalato)borate (LiDFOB).[109] Shi and coworkers also developed a similar electrolyte of 1 M lithium bis(oxalato) borate (LiBOB) in a novel blend of GBL with inert hydrofluoroether.[110] This unique combination proved effective across a wide temperature spectrum (−40 to 60 °C) in Gr‖NMC_{111} cells, which could still deliver 74 mA h g^{-1} at the low end of this range, but did not function at all with a conventional electrolyte (Fig. 13b and c). A follow-up study by the same group also demonstrated excellent safety and processability characteristics for a similar electrolyte containing LiDFOB.[111] Given these promising early results and the wealth of modern additive choices, it may be time to revisit GBL-based electrolytes as a serious option for next-generation LIBs.

Room-temperature ionic liquids. Room-temperature ionic liquids (RTILs or simply ILs) are a diverse group of materials widely studied for their unique physical, electrochemical and solvency properties. Many ILs have been proposed as components of LIB electrolytes, especially for improved safety and cyclability at high temperatures. However, in general, their high viscosities/melting points and poor wettability with commercial separators require that they be blended with organic solvents to achieve reasonable performance below 0 °C. For instance, Xiang and coworkers investigated electrolytes containing 0.1–0.4 mol kg^{-1} lithium bis(trifluoromethanesulfonyl)imide (LiTFSI) in *N*-methyl-*N*-propylpiperidinium bis(trifluoromethanesulfonyl)imide (PP_{13}TFSI) in Li‖$LiCoO_2$ half cells.[112] While this system performed quite well at room temperature and C/10 rate (137 mA h g^{-1} by cathode active weight), capacity dropped to 119 mA h g^{-1} at only 10 °C, and the cell became inoperable at lower temperatures due to freezing of the electrolyte. Addition of only 20 wt% DEC to the ionic liquid, however, reduced the liquidus temperature to −19 °C, while 40 wt% DEC suppressed crystallization altogether. All electrolytes were confirmed to be non-flammable. The 4 : 1 PP_{13}TFSI : DEC blend with 0.4 mol kg^{-1} LiTFSI allowed Li‖$LiCoO_2$ half cells to operate at −10 °C with 102 mA h g^{-1} capacity at C/10 rate – 72% of its room-temperature value.

An additional challenge facing RTILs is their general instability at low voltages. In order to intercalate and deintercalate lithium reversibly, low-potential anodes, *i.e.* graphite or lithium metal must form a dimensionally-stable SEI that prevents continuous decomposition. For graphite, ionic liquids based on the TFSI anion cannot accomplish this. However, many researchers have partially addressed the issue by adding significant amounts of the structurally-similar bis(fluorosulfonyl) imide (FSI) anion, which degrades rapidly to form inorganic protecting layers.[113] This strategy also tends to suppress crystallization and lower viscosity. Kunze *et al.* demonstrated that mixtures of *N*-butyl-*N*-methylpyrrolidinium (Pyr_{14}) TFSI and *N*-methyl-*N*-propylpyrrolidinium (Pyr_{13}) FSI have liquidus temperatures far below that of either parent compound (−18 °C and −8 °C, respectively).[114] The $(Pyr_{13}FSI)_{0.836}(Pyr_{14}TFSI)_{0.164}$ intermediate blend maintained a conductivity $>10^{-3}$ S cm^{-1} down to −20 °C, while $(Pyr_{13}FSI)_{0.568}(Pyr_{14}TFSI)_{0.432}$ remained liquid with conductivity 10^{-4} S cm^{-1} at −40 °C. These values are comparable to state-of-the-art organic electrolytes, although the relevance of this data may be limited, since none of the reported blends contained lithium and the lithium transference numbers of RTIL blends are generally quite low.[115] Yamagata *et al.* tested a mixed electrolyte of 0.45 M LiTFSI in 1-ethyl-3-methylimidazolium (EMIM) FSI in Li‖Gr half-cells, comparing the performance to a standard electrolyte (1 M $LiPF_6$ in EC/DMC 1 : 1 v/v).[116] The IL electrolyte outperformed the standard at rates up to 5C and temperatures from 25–60 °C, but was initially inoperable at 0 °C. However, a small amount of LiBOB additive dramatically improved the performance, allowing these cells to pass 67% of their room-temperature capacity after 25 cycles at 0 °C (C/10 rate).

Overall, the concept of low-temperature electrolytes based purely on ILs appears to have some potential, but more focused study would be required to realize competitive performance. When the additional drawbacks of IL electrolytes are factored in, such as high cost and low t_+, the outlook becomes discouraging, at least for this application space. We suggest that additional research might focus on IL/organic solvent mixtures rather than pure ILs. At least one existing study has validated this approach: Wang and coworkers found that 1 wt% $EMIMBF_4$ added to a standard EC/EMC electrolyte could nearly double the discharge capacity of Gr‖NMC_{523} pouch cells at −30 °C.[117] Furthermore, it remains to be seen whether the general trends discussed in this review still apply to a majority-ionic system, *e.g.* is charge transfer still the limiting step at low temperature, and is solvation structure still predictive of R_{ct} when the coordinating species are themselves charged? Further research into these fundamental questions is encouraged.

Other solvent types. The strong electron-donating properties of organosulfur compound tetrahydrothiophene-1-oxide (THTO) were taken advantage of by Oldiges and coworkers,

who blended this liquid in varying ratios with PC to form an electrolyte solvent base.[118] Combined experimental and simulation data indicated that THTO preferentially replaced PC in the solvation shell of Li^+, which was reduced to form a passivating SEI which prevented PC co-intercalation. When compared to a standard electrolyte (1 M $LiPF_6$ in EC/DEC 1 : 1 w/w), the mixed electrolyte 1 M $LiPF_6$ in THTO/PC 15 : 85 mol/mol roughly doubled the capacity of Gr‖NMC_{111} cells at 0 °C and 1C rate.

One extraordinarily unique low-temperature system comes from Rustomji *et al.*, who reported electrolytes based on liquefied gases.[119] Using a pressurized cell, these authors were able to dissolve 0.1 M LiTFSI in fluoromethane, a gas with a boiling point of −78 °C at 1 atm. Due to the extreme low viscosity of this material (owing to the weak interactions between molecules), the resulting electrolyte displayed high conductivity $\sim 10^{-3}$ S cm^{-1} across all temperatures from −60 °C to 25 °C, despite the comparatively low salt concentration. Addition of 5% CO_2 enabled formation of a stable SEI on lithium metal and allowed more salt to be dissolved. Li‖$LiCoO_2$ half cells cycled perfectly well in a liquefied gas electrolyte (0.2 M LiTFSI in fluoromethane/CO_2 19 : 1) down to −60 °C (60.6% capacity compared to room temperature) and performed similarly at 25 °C to 1 M $LiPF_6$ in EC/DEC 1 : 1 w/w. The same group recently followed up on this work using either tetrahydrofuran[120] or acetonitrile[121] as solvating additives to achieve higher salt concentrations and improved performance with lithium metal. It should be noted, of course, that the vapor pressures of these liquified gas solvents are multiple MPa under ordinary conditions, creating an inherent challenge to any practical application of this system.

Primary salts

No LIB can function without a lithium-containing electrolyte to transport Li^+ across the cell interior and, when it comes to sources of dissociable lithium, $LiPF_6$ is the undisputed first choice. It has been said that $LiPF_6$ earned this position not due to any one outstanding property, but rather due to its lack of any crippling disadvantages.[13] That being said, non-PF_6^- salts can – and have – been utilized in application-specific LIBs, where they may provide certain upside. For example, different salts may have better solubility in non-typical solvents or participate in the passivation of electrode interfaces. These characteristics can be leveraged to the benefit of low-temperature performance. Salt formulations investigated by the references cited here may be found summarized in Table 3 along with their structures.

Borates ($LiBF_4$, LiBOB, LiDFOB). Zhang, Xu and Jow reported as early as 2002 that $LiBF_4$ could enable better cell performance than $LiPF_6$ at sub-zero temperatures, despite poorer ionic conductivity and SEI characteristics in its electrolytes.[122] Subsequent analysis by these authors found a dramatic reduction in full-cell R_{ct} when $LiBF_4$ was used (Fig. 14a),[123] although to our knowledge the chemical mechanism behind this effect has yet to be clarified.

Unfortunately, $LiBF_4$ has not gained widespread popularity as a primary salt due to the inadequate SEI formed in its electrolyte solutions, which precludes extended cycling. On the other hand, lithium bis(oxolato)borate (LiBOB) has received steady investigation precisely because of its SEI-forming abilities, which may reduce or eliminate the need for EC solvent.[124] Naturally, this has attracted interest for low-temperature electrolyte designs,[110,125,126] where it is desirable to minimize EC content. However, LiBOB comes with its own set of drawbacks, including poorer solubility and conductivity than $LiPF_6$, which limit its applications as well. Kang Xu has explored the topic of LiBOB electrolyte design in more detail elsewhere.[127]

An appropriate compromise can be found in lithium difluoro(oxolato)borate (LiDFOB), which shares the SEI-forming characteristics of LiBOB, but with improved solubility and ion dissociation characteristics. This salt has proven to be suitable for a wide range of electrolyte designs,[128] including lactone-based formulations.[109,111] Several groups have reported that a mixed-salt approach – using LiDFOB together with $LiBF_4$ – can maximize the advantages of both compounds at low temperature. For instance, Li *et al.* investigated an EC/DMS/EMC 1 : 1 : 3 v/v electrolyte containing 0.9 M total of LiDFOB and $LiBF_4$ in a 5.365 : 1 mass ratio.[77] These authors found the ionic conductivity of this mixture to be similar to that a traditional $LiPF_6$-based blend across the temperature range −40 to 20 °C. Importantly, the electrolyte was found to be compatible with both graphite and $LiFePO_4$ in half-cell tests, enabling drastically-higher capacities than the control electrolyte at −20 °C (Fig. 14b). Zhou and coworkers conducted a detailed study of similar electrolytes (1 M salt in EC/DMC/EMC 1 : 1 : 1 w/w) with varying DFOB/BF_4 ratio across the range −20 to 60 °C.[129] Pure LiDFOB performed universally best at room temperature and higher, producing the best conductivity and discharge capacity in Gr‖LMNO cells, but this trend was exactly reversed at −20 °C, with blends showing intermediate properties (Fig. 14c). An ideal balance was struck at 0.8 M LiDFOB and 0.2 M $LiBF_4$, since even a relatively small amount of $LiBF_4$ was found to reduce cell R_{ct} from 482.6 Ω to 346.3 Ω at −20 °C, without compromising the effective passivation of LiDFOB. As a result, cells containing this blend showed excellent capacity retention across all temperatures.

Sulfonylimides (LiTFSI, LiFSI, LiBETI). Most of the sparse literature on $LiPF_6$-free electrolytes below 0 °C has focused on borate salts, with other structures proving to be quite rare. Nonetheless, exceptions do exist, mostly when unique solvents are involved, *e.g.* the IL-based,[112,114,116] ester-based[107] or highly-fluorinated electrolytes[94] described in sections above. These designs exploit the high solubility, dissociation ability and chemical stability of lithium sulfonylimide salts (LiTFSI, LiFSI, LiBETI, *etc.*) – as well as the interface-stabilizing characteristics of LiFSI[113] – in situations where $LiPF_6$ is unsuitable. Mandal and coworkers did publish an article in 2006 which directly compares LiTFSI to $LiPF_6$ (0.9 M salt in EC/DMC/EMC 15 : 37 : 48 w/w) across various temperatures.[130] Most interestingly, the LiTFSI electrolyte showed nearly an order-of-magnitude reduction in charge-transfer resistance on lithium metal at 30 °C, although no measurements were done at lower temperatures.

Table 3 Primary salt summary table

Primary salt	Electrolyte	Ref.
$LiBF_4$ 	0.9 M LiDFOB/$LiBF_4$ (5.4 : 1 w/w), EC/DMS/EMC (1 : 1 : 3 v/v)	77
	1 M $LiBF_4$, PC/EMC/MB/EC (19 : 19 : 57 : 5 w/w)	106
	1 M $LiBF_4$, PC/EC/EMC (1 : 1 : 3 w/w)	122
	1 M $LiBF_4$, EC/DMC/DEC (1 : 1 : 1 w/w)	123
	1 M $LiBF_4$, EC/DMC/GBL (1 : 1 : 1 w/w)	125
	1 M LiDFOB/$LiBF_4$ (4 : 1 mol/mol), DMC/EC/EMC (1 : 1 : 1 w/w)	129
	1 M LiDFOB/$LiBF_4$ (1 : 1 mol/mol), DMC/EC/EMC (1 : 1 : 1 w/w)	
	1 M LiDFOB/$LiBF_4$ (1 : 4 mol/mol), DMC/EC/EMC (1 : 1 : 1 w/w)	
	1 M $LiBF_4$, DMC/EC/EMC (1 : 1 : 1 w/w)	
LiBOB 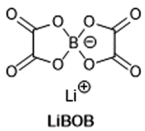	1 M LiBOB, GBL	
	1 M LiBOB, GBL/DMC (7 : 3 w/w)	110
	1 M LiBOB, GBL/F-EPE (7 : 3 w/w)	
	1 M LiBOB, EC/EMC (1 : 1 w/w)	125
	1 M LiBOB, PC/EC/EMC (1 : 1 : 3 w/w)	
	See patent text	126
LiDFOB 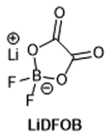	0.9 M LiDFOB/$LiBF_4$ (5.4 : 1 w/w), EC/DMS/EMC (1 : 1 : 3 v/v)	77
	1 M LiDFOB, EC/DMC/DEC (1 : 1 : 1 v/v)	109
	1 M LiDFOB, GBL/MB (1 : 1 v/v)	
	1 M LiDFOB, GBL/F-EPE (7 : 3 w/w)	111
	1 M LiDFOB, PC/EC/EMC (3 : 3 : 4 w/w)	128
	1 M LiDFOB, DMC/EC/EMC (1 : 1 : 1 w/w)	129
	1 M LiDFOB/$LiBF_4$ (4 : 1 mol/mol), DMC/EC/EMC (1 : 1 : 1 w/w)	
	1 M LiDFOB/$LiBF_4$ (1 : 1 mol/mol), DMC/EC/EMC (1 : 1 : 1 w/w)	
	1 M LiDFOB/$LiBF_4$ (1 : 4 mol/mol), DMC/EC/EMC (1 : 1 : 1 w/w)	
LiTFSI 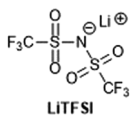	2 M LiTFSI, EA	107
	0.1 M LiTFSI, CH_3F/CO_2 (19 : 1 w/w)	119
	0.2 M LiTFSI, CH_3F/CO_2 (19 : 1 w/w)	
	0.3 M LiTFSI, 0.3 M THF, CH_3F/CO_2 (19 : 1 w/w)	120
	0.9 M LiTFSI, EC/DMC/EMC (15 : 37 : 48 w/w)	130
	21 m LiTFSI, H_2O	131
	21 m LiTFSI, H_2O + 9.25 m LiTFSI, DMC	
	15.3 m LiTFSI, H_2O/AN (1 : 1 mol/mol)	
	Composition series, see text	132
	5.2 m LiTFSI, H_2O	133
LiBETI 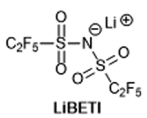	0.7 M LiBETI, FEC/DEC/M3 (1 : 5 : 14 v/v)	94
LiFSI 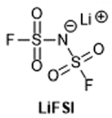	4.2 M LiFSI, FEC/FEMC (1 : 2 v/v)	
	1.28 M LiFSI, FEC/FEMC/D2 (1 : 2 : 7 v/v)	
		94

Since charge-transfer resistance is generally the limiting factor in LIB cells under sub-zero conditions, this observation could prove relevant. Li‖$LiNi_{0.8}Co_{0.2}O_2$ half cells and Gr‖$LiNi_{0.8}Co_{0.2}O_2$ full cells were also demonstrated to operate well in the LiTFSI-containing electrolyte, with the half cells remaining functional down to −40 °C. More recently, several independent studies have reported "water-in-salt" electrolytes based on lithium sulfonylimides with low-temperature operability as a key selling point.[131–133] Overall, LiTFSI and its related compounds appear to be underutilized in low-temperature LIB literature, and it is our opinion that the field could benefit by adding this class of materials to its toolbox. Potential investigators should be warned, however, that these salts may cause severe corrosion to Al current collectors unless additional passivating strategies are employed.[134]

A note on silicon anodes

Although graphite has been the anode of choice for virtually the entire commercial history of LIBs, future designs are likely to rely on some combination of silicon and carbon due to the former's high specific capacity, earth abundance and mature commercial production. The various characteristics and challenges of silicon and Si/C composite anodes under "ordinary" operating conditions have been covered elsewhere extensively.[64,135–137] Curiously, however, we were only able to locate a handful of reports that directly address silicon performance at low temperatures. One of the earliest reports came in 2005 from Kasavajjula and Wang, who developed a composite anode containing graphite and nano-Si in a 5 : 1 ratio, along with a solid electrolyte filler and PEO-$LiClO_4$ binder.[138] In half cells with lithium metal and an electrolyte of 1 M $LiPF_6$ in

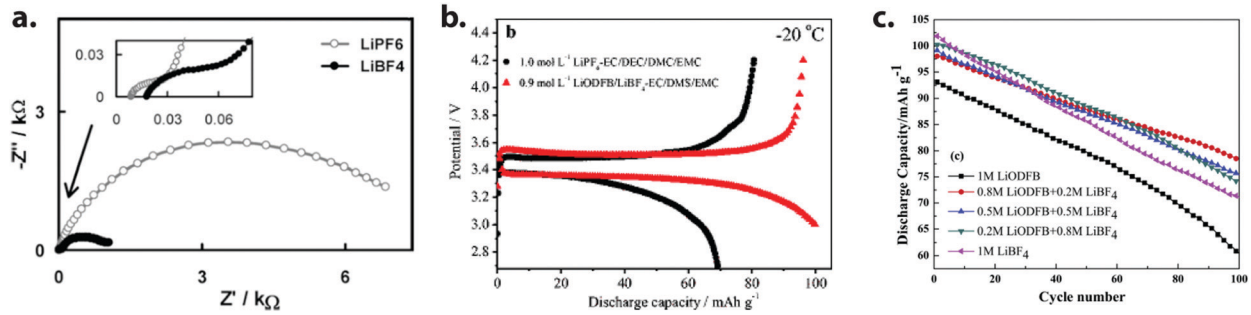

Fig. 14 (a) Impedance spectra at −20 °C of fully-charged Li-ion cells containing 1 molal $LiPF_6$ in EC/DMC/DEC 1 : 1 : 1 w/w, compared to 1 molal $LiBF_4$ in the same solvent mixture. Charge-transfer resistance is significantly reduced in the $LiBF_4$-based electrolyte. Reprinted by permission from Springer Nature: ref. 123, copyright 2002. (b) Initial −20 °C charge/discharge curves of Li‖$LiFePO_4$ cells with a mixed LiDFOB/$LiBF_4$ electrolyte *versus* a standard mixture. The discharge rate is 0.5C. Reprinted by permission from Springer Nature: ref. 77, copyright 2014. (c) Cycling performance of Gr|$LiNi_{0.5}Mn_{1.5}O_4$ cells at −20 °C in electrolytes containing varying ratios of LiDFOB to $LiBF_4$, with 1 M total salt in EC/DMC/EMC 1 : 1 : 1 w/w. A combination of 0.8 M LiDFOB and 0.2 M $LiBF_4$ strikes the best balance between initial capacity and retention. Reprinted from ref. 129 with permission from Elsevier.

EC/DMC/DEC/EMC 1 : 1 : 1 : 3, this electrode was found to reversibly store 321 mA h g^{-1} at 25 °C, with moderate retention of 277 mA h g^{-1} at −10 °C and 222 mA h g^{-1} at −20 °C. Further lowering the temperature caused more dramatic losses, with 160 mA h g^{-1} available at −30 °C and only 84 mA h g^{-1} at −40 °C. Careful impedance analysis led the authors to conclude that increasing charge-transfer resistance was responsible for the capacity loss below −20 °C, although the inclusion of solid electrolyte helped this situation significantly compared to a control electrode without it.

Several more articles have been published on this topic within the past five years as silicon has inched closer to widespread adoption. Markevitch, Salitra and Aurbach compared the performance of monolithic amorphous silicon (a-Si) anodes (capacity-limited to 600 mA h g^{-1} lithiation) to graphite counterparts of identical areal capacity, using half cells with

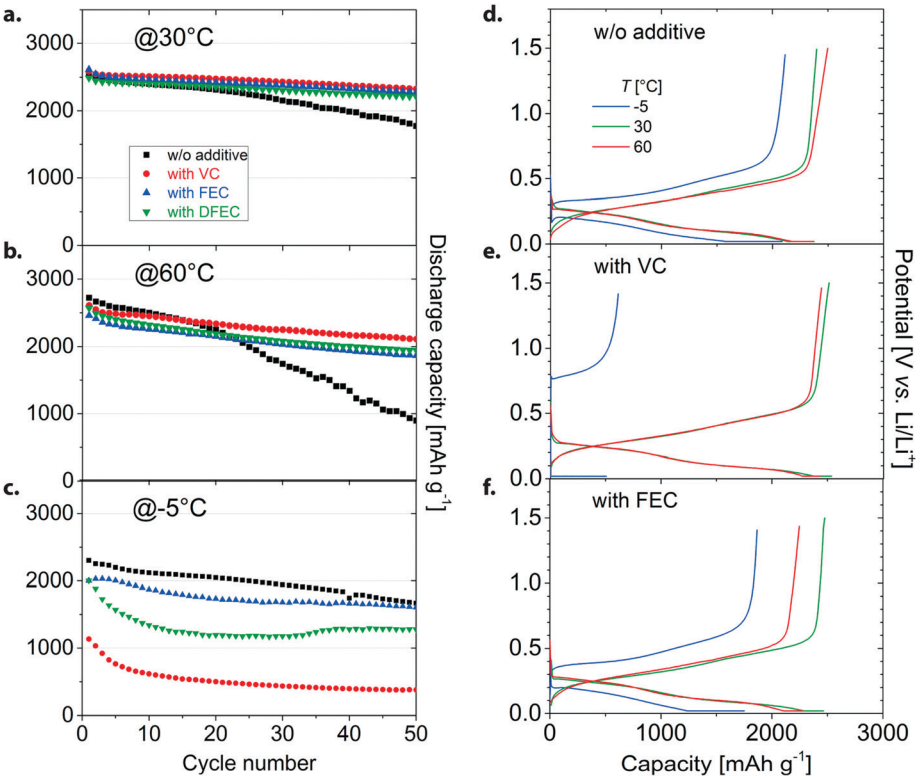

Fig. 15 (a–c) Cycling performance of Si nanoflake powder half-cells containing various electrolytes at varying temperatures. The base electrolyte was 1 M $LiPF_6$ in EC/DEC 1 : 1 v/v, with 10 wt% "additive" compounds as indicated. FEC appears to offer the best trade-off between high-temperature stability and low-temperature discharge capacity. (d and e) 10th cycle charge and discharge curves for the above cells at different temperatures. While VC-added electrolyte produces the best capacity (by a small amount) at 25 °C and 60 °C, it creates extreme polarization in the cell at −5 °C. Both FEC and VC additives appear to increase cell resistance at sub-zero conditions relative to the base electrolyte. Reprinted from ref. 93 with permission from Elsevier.

1 M $LiPF_6$ in FEC/DMC (1 : 4 w/w) electrolyte.[139] Following lithiation at 30 °C, the delithiation capacity of a-Si exhibited virtually no temperature dependence down to −30 °C; furthermore, the silicon anodes could be charged and discharged under such conditions with no observable capacity drop, while graphite lost capacity rapidly when charged at 0 °C and below. Haruta *et al.* compared the effects of several common electrolyte additives on Si nanoflake anodes over a wide temperature range (Fig. 15),[93] finding 10 wt% FEC to be the most effective at −5 °C and moderately effective at 60 °C. In contrast, 10 wt% VC produced slightly better capacity at high temperature, but drastically reduced capacity at sub-zero temperature.

Notably, all of the above studies derived their conclusions from half cells with lithium metal. In contrast, two articles published just months prior to this writing examined commercial large-format cells containing Si or Si/Gr anodes paired with NCA cathodes. Subburaj and coworkers studied 1 A h pouch cells made from sputter-deposited Si anodes and a conventional electrolyte blend (1 M $LiPF_6$ in EC : DMC : DEC 1 : 3 : 1 v/v).[140] These cells retained an impressive 65.3% of their 20 °C discharge capacity at −40 °C; however, capacity faded rapidly after 40 low-temperature charge/discharge cycles. Notably, the authors identified cathode structural transformation as the cause of this degradation, rather than lithium plating or other anode processes. Richter and coworkers took a different approach, examining minor-Si-content (3.5 wt%) anodes in 18 650 format cylindrical cells with *operando* neutron diffraction.[141] This experiment revealed that, under low-temperature charge conditions, graphite was lithiated more rapidly than silicon despite its lower potential, indicating a kinetic limitation that may be a target for future optimization.

Doubtless, many questions remain about the characteristics of silicon anodes below 0 °C, indicating that this area is ripe for further investigation. We observe that – generally speaking – silicon has been reported to resist low-temperature capacity loss better than graphite, an advantage also shared by the related alloy-type material tin.[142] However, it remains to be seen whether this is an intrinsic benefit, or merely a result of different particle shapes/sizes, electrode fabrication methods and testing protocols. We strongly encourage additional research in this area. Results from the various references cited here are summarized in Table 4.

Summary and outlook

The future of lithium-ion batteries (LIBs) will require them to fill more roles than ever before and do so across a wider range of operating temperatures. It is well-known that the available discharge capacity of lithium-ion cells (even when charged at room temperature) tends to drop off considerably below −20 °C, which poses a significant challenge for applications in aerospace and transportation where sub-zero ambient conditions are common. This is largely due to a massive increase to internal resistance as the temperature is lowered. Solving the issue of low-temperature performance requires careful consideration of the many simultaneous chemical processes occurring within a lithium-ion cell, each of which contributes an associated impedance. Often, the best way to address this complex problem is by way of the one component which affects nearly every internal process: the non-aqueous liquid electrolyte.

In this review, we first summarized the many individual sources of impedance that are associated with liquid electrolytes and the role that they play in low-temperature performance. A typical lithium-ion electrolyte consists of 1 M $LiPF_6$ dissolved in a liquid mixture of ≤50% ethylene carbonate (EC) along with linear carbonates (DMC, DEC, EMC) and a few wt% of additives (*e.g.* FEC, VC). While the bulk physical properties of these formulations, *e.g.* ionic conductivity, have been well-studied due to their importance at moderate-to-high temperatures and/or high currents, low-temperature performance does not generally correlate with bulk conductivity. If anything, the most relevant physical property is instead liquidus point, where solids begin to block electrode pores and reduce ion access to active surfaces. However, by far the biggest limiting factor in sub-zero LIB operation is charge-transfer resistance, a process that has been linked by several studies to Li^+ desolvation at the electrolyte/active material interface. These large desolvation energies and high freezing points are both largely due to the use of EC, which is a high-melting compound (36 °C) that possesses the large dielectric permittivity (ε = 90 at 40 °C) necessary to dissociate lithium salts from their counterions. EC is also indispensable because of its ability to passivate graphite anode surfaces upon reductive breakdown, forming a solid–electrolyte interphase (SEI) that stops further electrolyte decomposition and stabilizes the carbon structure to exfoliation upon repeated cycling. While the SEI (and its thinner cathode counterpart, the CEI) do indeed contribute some impedance to the cell, evidence suggests that interphasial ion transport is not the primary limit on low-temperature performance. Rather, the importance of SEI comes from its ability to prevent capacity loss *via* parasitic corrosion current, which is critical at all temperatures and becomes especially challenging when attempting to reduce EC content in the electrolyte. Attempting to charge a LIB under sub-zero conditions also introduces new capacity loss mechanisms associated with lithium deposition at low anode potentials.

Just as the causes of low-temperature capacity loss are multifaceted, so too are the potential strategies to address them *via* electrolyte engineering. We have concisely summarized recent developments in this area, which can be broken down into three primary research thrusts: additives, solvents and salts. Successful electrolyte additives generally assist in the formation of robust SEI/CEI layers with low resistance to Li^+ transport, which reduces reliance on EC as a main solvent component. Studied additives include molecular compounds like fluoroethylene carbonate (FEC), tris(trimethylsilyl)phosphite (TMSPi) and sulfur compounds in a variety of oxidation states, *e.g.* dimethyl sulfite (DMS) and 1,3,2-dioxathiolane-2,2-dioxide (DTD). Ionic compounds may also fill this role, including novel lithium salts like $LiPO_2F_2$ or even non-lithium-containing salts such as $CsPF_6$. Alternately or in combination with additives, many authors have sought to augment or replace traditional solvents as well.

Table 4 Silicon anode summary table

Cathode‖anode	Electrolyte	Temperature (°C)	Discharge capacity (mA h g^{-1})	Capacity retention (% of RT)	Rate	Notes	Ref.
a-Si nanoflakes‖Li	1 M $LiPF_6$, EC/DEC (1 : 1 v/v)	−5	2100	84%	n/a	Capacity estimated after 10 cycles at low temperature	93
	1 M $LiPF_6$, EC/DEC (1 : 1 v/v) + 10% VC		600	25%			
	1 M $LiPF_6$, EC/DEC (1 : 1 v/v) + 10% FEC		1900	79%			
	1 M $LiPF_6$, EC/DEC (1 : 1 v/v) + 10% DFEC		1300	54%			
Si/Gr‖Li	1 M $LiPF_6$, EC/DEC/DMC/EMC (1 : 1 : 1 : 3 v/v)	−10	277	86%	5 mA g^{-1}	10% nano-Si, polymer/ ceramic composite binder	138
		−20	222	69%			
		−30	160	50%			
		−40	84	26%			
a-Si nanopillars‖Li	1 M $LiPF_6$, FEC/DMC (1 : 4 w/w)	0	600	100%	0.24 mA c^{-1} m^{-2}	Capacity-limited to 600 mA h g^{-1} charge	139
		−10	600	100%			
		−20	600	100%			
		−30	600	100%			
NCA‖Si	1 M $LiPF_6$, EC/DMC/DEC (1 : 3 : 1 v/v) + 60% EA + 10% FEC	−40	707 (mA h)	65%	C/10	Sputtered Si, pouch cell	140
NCA‖Si/Gr	n/a	−21	2.03 (A h, charge)	81%	0.1C	3.5 wt% Si, pouch cell, mechanistic study	141
			1.71 (A h, charge)	69%	0.5C		
			1.16 (A h, charge)	47%	0.75C		
Nano-Sn/Gr‖Li	1 M $LiPF_6$, EC/DMC (1 : 1 v/v)	−20	195	30%	65 mA g^{-1}	Sn nanoparticles embedded in expanded graphite	142
			130	20%	130 mA g^{-1}		

One of the simplest, but most effective, solvent components at low temperature is propylene carbonate (PC), which shares many characteristics of EC, but with a lower melting point (−49 °C). Modern additive developments have made it possible to partially or entirely replace EC with PC without causing undesirable breakdown of graphite, as known from the early days of LIB research. FEC and vinylene carbonate (VC) have also been explored as major solvent components. However, many researchers have turned to another class of solvents entirely: esters, which possess low melting points and low viscosities, while being of moderately polar character. On the other hand, low-molecular-weight esters are often detrimentally unstable at low anode potentials; an exhaustive study has found methyl propionate (MP) to possess the best trade-off in properties, although protective additives or higher-potential anodes like $Li_4Ti_5O_{12}$ (LTO) can eliminate stability concerns. The cyclic ester gamma-butyrolactone (GBL) has also shown great potential as a replacement for chemically-similar EC. Other creative solvents include room-temperature ionic liquids (RTILs) and liquified gases, *i.e.* fluoromethane contained under pressure. Finally, other investigators have turned away from the ubiquitous $LiPF_6$ in favor of other lithium salts. In particular, borates have received significant attention due to the discovery of vastly-reduced charge-transfer resistance in $LiBF_4$-based electrolytes at low temperatures. Recently, lithium bis(oxalate) borate (LiBOB) and lithium difluoro(oxalato)borate (LiDFOB) have been characterized for sub-zero applications and been found to possess intriguing advantages. Other salts like lithium bis(trifluoromethane)sulfonylimide (LiTFSI), while well-characterized in other contexts, have received comparatively little investigation at low temperature.

Finally, we would like to conclude by pointing out several emerging areas of research for low-temperature LIB electrolytes which deserve greater attention. The most obvious of these is in silicon-based anode materials, which have seen increasing commercial attention in combination with graphite and are likely to entirely replace graphite at some point in the future. Despite the explosion of silicon research over the past decade, there have been remarkably few published reports on Si anodes at low temperatures. It remains to be seen how the "conventional wisdom" enumerated in this review will apply to Si materials systems, especially since the anode is generally considered to be the dominating factor when it comes to sub-zero battery operation. Additionally, there are many electrolyte components which, for one reason or another, were deemed unsuitable during the early days of LIB research, despite marked advantages at low temperature. A perfect example is PC, which cannot form a protective SEI on its own, but is now enjoying a revival due to the advent of sacrificial additives. GBL, on the other hand, has yet to experience such renewed interest, despite several promising recent results, especially in combination with borate salts like LiDFOB for which GBL seems to exhibit a particular synergy. It should also be mentioned that fluorine-containing solvents, especially hydrofluoroethers, have (deservedly) enjoyed recent popularity as electrolyte components for a variety of applications.[94,110,143–145] While a handful of these reports have addressed sub-zero performance, this angle remains underexplored given their tendencies towards wide liquid range and low Li^+ solvation energy. In general, while incremental progress remains possible, the most exciting developments in low-temperature LIB performance have often come from the most novel design strategies, such as highly-fluorinated electrolytes, liquefied gases or non-lithium metallic salt additives. With a greater commitment to push the envelope on electrolyte development, we can expect a bright future for batteries that will carry us down the road, across the sky, through space and to the limits of human imagination.

List of abbreviations

AN	Acetonitrile
BB	Butyl butyrate
BETI	Bis(pentafluoroethanesulfonyl)imide
BOB	Bis(oxalato)borate
BuS	Butyl sultone
CEI	Cathode-electrolyte interphase
CMDO	4-Chloromethyl-1,3,2-dioxathiolane-2-oxide
D2	Tetrafluoro-1-(2,2,2-trifluoroethoxy)ethane
DEC	Diethyl carbonate
DFEC	Difluoroethylene carbonate
DMC	Dimethyl carbonate
DMS	Dimethyl sulfite
DFBOP	Difluorobis(oxolato)phosphate
DFOB	Difluoro(oxalato)borate
DTD	1,3,2-Dioxathiolane-2,2-dioxide
EA	Ethyl acetate
EB	Ethyl butyrate
EC	Ethylene carbonate
EIS	Electrochemical impedance spectroscopy
EMC	Ethyl methyl carbonate
EMIM	1-Ethyl-3-methylimidazolium
EP	Ethyl propionate
ETFA	Ethyl trifluoroacetate
FEC	Fluoroethylene carbonate
FEMC	2,2,2-Trifluoroethyl methyl carbonate
F-EPE	1,1,2,2-Tetrafluoroethyl-2,2,3,3-tetrafluoropropyl ether
FI	Fluorosulfonyl isocyanate
FSI	Bis(fluorosulfonyl)imide
GBL	Gamma-butyrolactone
Gr	Graphite
IL	Ionic liquid
LIB	Lithium-ion battery
LTO	$Li_4Ti_5O_{12}$
M3	Methoxyperfluorobutane
MA	Methyl acetate
MB	Methyl butyrate
MCMB	Mesocarbon microbead (graphite)
MEC	Methylene ethylene carbonate
MP	Methyl propionate
MPFP	Methyl pentafluoropropionate
NCA	$LiNi_{0.8}Co_{0.15}Al_{0.05}O_2$
NMC_{xyz}	$LiNi_{0.x}Mn_{0.y}Co_{0.z}O_2$
PB	Propyl butyrate
PC	Propylene carbonate
PCS	1,3-Propanediol cyclic sulfate
PES	Prop-1-ene-1,3-sultone
PP_{13}	*N*-Methyl-*N*-propylpiperidinium
PS	1,3-Propane sultone
Pyr_{13}	*N*-Methyl-*N*-propylpyrrolidinium
Pyr_{14}	*N*-Butyl-*N*-methylpyrrolidinium
R_{bulk}	Bulk electrolyte ionic resistance
R_{ct}	Charge-transfer resistance
R_{SEI}	SEI ionic resistance
SEI	Solid–electrolyte interphase
TDI	2-Trifluoromethyl-4,5-dicyanoimidazole
TFEA	2,2,2-Trifluoroethyl acetate
TFEB	2,2,2-Trifluoroethyl butyrate
TFENH	2,2,2-Trifluoroethyl *n*-caproate
TFSI	Bis(trifluoromethanesulfonyl)imide
THF	Tetrahydrofuran
THTO	Tetrahydrothiophene-1-oxide
TMSPi	Tris(trimethylsilyl)phosphite
VC	Vinylene carbonate
XPS	X-ray photoelectron spectroscopy

Conflicts of interest

There are no conflicts to declare.

Acknowledgements

This research was supported by the Assistant Secretary for Energy Efficiency and Renewable Energy, Office of Vehicle Technologies of the U.S. Department of Energy under Contract No. DE-AC02-05CH11231.

References

1 M. C. Smart, B. V. Ratnakumar, R. C. Ewell, S. Surampudi, F. J. Puglia and R. Gitzendanner, *Electrochim. Acta*, 2018, **268**, 27–40.
2 T. Chen, Y. Jin, H. Lv, A. Yang, M. Liu, B. Chen, Y. Xie and Q. Chen, *Trans. Tianjin Univ.*, 2020, **26**, 208–217.
3 L. Trahey, F. R. Brushett, N. P. Balsara, G. Ceder, L. Cheng, Y.-M. Chiang, N. T. Hahn, B. J. Ingram, S. D. Minteer, J. S. Moore, K. T. Mueller, L. F. Nazar, K. A. Persson, D. J. Siegel, K. Xu, K. R. Zavadil, V. Srinivasan and G. W. Crabtree, *Proc. Natl. Acad. Sci. U. S. A.*, 2020, **117**, 12550–12557.
4 M. Chen, Y. Zhang, G. Xing, S. L. Chou and Y. Tang, *Energy Environ. Sci.*, 2021, **14**, 3323–3351.
5 T. M. Bandhauer, S. Garimella and T. F. Fuller, *J. Electrochem. Soc.*, 2011, **158**, R1.
6 M.-T. F. Rodrigues, G. Babu, H. Gullapalli, K. Kalaga, F. N. Sayed, K. Kato, J. Joyner and P. M. Ajayan, *Nat. Energy*, 2017, **2**, 17108.
7 T. Ould Ely, D. Kamzabek and D. Chakraborty, *Front. Energy Res.*, 2019, **7**, 71.
8 P. V. Chombo and Y. Laoonual, *J. Power Sources*, 2020, **478**, 228649.
9 R. Fong, U. von Sacken and J. R. Dahn, *J. Electrochem. Soc.*, 1990, **137**, 2009–2013.
10 P. Jehnichen, K. Wedlich and C. Korte, *Sci. Technol. Adv. Mater.*, 2019, **20**, 1–9.
11 A. Tomaszewska, Z. Chu, X. Feng, S. O'Kane, X. Liu, J. Chen, C. Ji, E. Endler, R. Li, L. Liu, Y. Li, S. Zheng, S. Vetterlein, M. Gao, J. Du, M. Parkes, M. Ouyang,

M. Marinescu, G. Offer and B. Wu, *eTransportation*, 2019, **1**, 100011.
12 S. Hess, M. Wohlfahrt-Mehrens and M. Wachtler, *J. Electrochem. Soc.*, 2015, **162**, A3084–A3097.
13 K. Xu, *Chem. Rev.*, 2004, **104**, 4303–4417.
14 M. Petzl, M. Kasper and M. A. Danzer, *J. Power Sources*, 2015, **275**, 799–807.
15 Q. Li, D. Lu, J. Zheng, S. Jiao, L. Luo, C. M. Wang, K. Xu, J. G. Zhang and W. Xu, *ACS Appl. Mater. Interfaces*, 2017, **9**, 42761–42768.
16 R. Payne and I. E. Theodorou, *J. Phys. Chem.*, 1972, **76**, 2892–2900.
17 B. Schäffner, F. Schäffner, S. P. Verevkin and A. Börner, *Chem. Rev.*, 2010, **110**, 4554–4581.
18 M. S. Ding, K. Xu, S. S. Zhang, K. Amine, G. L. Henriksen and T. R. Jow, *J. Electrochem. Soc.*, 2001, **148**, A1196.
19 M. S. Ding, K. Xu and T. R. Jow, *J. Electrochem. Soc.*, 2000, **147**, 1688.
20 J. M. Tarascon and D. Guyomard, *Solid State Ionics*, 1994, **69**, 293–305.
21 E. J. Plichta and W. K. Behl, *J. Power Sources*, 2000, **88**, 192–196.
22 K. B. Oldham and J. C. Myland, *Fundamentals of Electrochemical Science*, Academic Press, San Diego, CA, 1994.
23 K. M. Diederichsen, E. J. McShane and B. D. McCloskey, *ACS Energy Lett.*, 2017, **2**, 2563–2575.
24 P. Barai, K. Higa and V. Srinivasan, *Phys. Chem. Chem. Phys.*, 2017, **19**, 20493–20505.
25 A. Ehrl, J. Landesfeind, W. A. Wall and H. A. Gasteiger, *J. Electrochem. Soc.*, 2017, **164**, A826–A836.
26 I. Villaluenga, D. M. Pesko, K. Timachova, Z. Feng, J. Newman, V. Srinivasan and N. P. Balsara, *J. Electrochem. Soc.*, 2018, **165**, A2766–A2773.
27 J. Landesfeind, H. A. Gasteiger, J. E. Soc and J. Landesfeind, *J. Electrochem. Soc.*, 2019, **166**, A3079.
28 L. O. Valoen and J. N. Reimers, *J. Electrochem. Soc.*, 2005, **152**, A882.
29 A. Nyman, M. Behm and G. Lindbergh, *Electrochim. Acta*, 2008, **53**, 6356–6365.
30 H. Lundgren, M. Behm and G. Lindbergh, *J. Electrochem. Soc.*, 2015, **162**, A413–A420.
31 S. S. Zhang, K. Xu and T. R. Jow, *Electrochim. Acta*, 2004, **49**, 1057–1061.
32 R. Jow, S. S. Zhang, K. Xu and J. Allen, *ECS Transactions*, ECS, 2007, vol. 3, pp. 51–58.
33 D. P. Abraham, J. R. Heaton, S.-H. Kang, D. W. Dees and A. N. Jansen, *J. Electrochem. Soc.*, 2008, **155**, A41.
34 K. Xu, A. Von Cresce and U. Lee, *Langmuir*, 2010, **26**, 11538–11543.
35 J. Li, C. F. Yuan, Z. H. Guo, Z. A. Zhang, Y. Q. Lai and J. Liu, *Electrochim. Acta*, 2012, **59**, 69–74.
36 A. Lewandowski, M. Biegun, M. Galinski and A. Swiderska-Mocek, *J. Appl. Electrochem.*, 2013, **43**, 367–374.
37 M. C. Smart, *J. Electrochem. Soc.*, 1999, **146**, 486.
38 B. Liu, Q. Li, M. H. Engelhard, Y. He, X. Zhang, D. Mei, C. Wang, J. G. Zhang and W. Xu, *ACS Appl. Mater. Interfaces*, 2019, **11**, 21496–21505.
39 X. Yu and A. Manthiram, *Energy Environ. Sci.*, 2018, **11**, 527–543.
40 Y. Chu, Y. Shen, F. Guo, X. Zhao, Q. Dong, Q. Zhang, W. Li, H. Chen, Z. Luo and L. Chen, *Electrochem. Energy Rev.*, 2020, **3**, 187–219.
41 C. Fang, Z. Liu, J. Lau, M. Elzouka, G. Zhang, P. Khomein, S. Lubner, P. N. Ross and G. Liu, *J. Electrochem. Soc.*, 2020, **167**, 020506.
42 T. Waldmann, B.-I. Hogg and M. Wohlfahrt-Mehrens, *J. Power Sources*, 2018, **384**, 107–124.
43 Y. Liu, Y. Zhu and Y. Cui, *Nat. Energy*, 2019, **4**, 540–550.
44 K. G. Gallagher, D. W. Dees, A. N. Jansen, D. P. Abraham and S.-H. Kang, *J. Electrochem. Soc.*, 2012, **159**, A2029–A2037.
45 C. Uhlmann, J. Illig, M. Ender, R. Schuster and E. Ivers-Tiffée, *J. Power Sources*, 2015, **279**, 428–438.
46 T. Waldmann, B.-I. Hogg, M. Kasper, S. Grolleau, C. G. Couceiro, K. Trad, B. P. Matadi and M. Wohlfahrt-Mehrens, *J. Electrochem. Soc.*, 2016, **163**, A1232–A1238.
47 E. J. McShane, A. M. Colclasure, D. E. Brown, Z. M. Konz, K. Smith and B. D. McCloskey, *ACS Energy Lett.*, 2020, **5**, 2045–2051.
48 B. V. Ratnakumar and M. C. Smart, *ECS Trans.*, 2010, **25**, 241–252.
49 M. Petzl and M. A. Danzer, *J. Power Sources*, 2014, **254**, 80–87.
50 B. Ng, P. T. Coman, E. Faegh, X. Peng, S. G. Karakalos, X. Jin, W. E. Mustain and R. E. White, *ACS Appl. Energy Mater.*, 2020, **3**(4), 3653–3664.
51 T. Waldmann, M. Wilka, M. Kasper, M. Fleischhammer and M. Wohlfahrt-Mehrens, *J. Power Sources*, 2014, **262**, 129–135.
52 N. Ghanbari, T. Waldmann, M. Kasper, P. Axmann and M. Wohlfahrt-Mehrens, *J. Phys. Chem. C*, 2016, **120**, 22225–22234.
53 I. D. Campbell, M. Marzook, M. Marinescu and G. J. Offer, *J. Electrochem. Soc.*, 2019, **166**, A725–A739.
54 Z. M. Konz, E. J. Mcshane and B. D. Mccloskey, *ACS Energy Lett.*, 2020, **15**, 41.
55 C. Vidal, O. Gross, R. Gu, P. Kollmeyer and A. Emadi, *IEEE Trans. Veh. Technol.*, 2019, **68**, 4560–4572.
56 Y. Ji and C. Y. Wang, *Electrochim. Acta*, 2013, **107**, 664–674.
57 S. Hein, T. Danner, D. Westhoff, B. Prifling, R. Scurtu, L. Kremer, A. Hoffmann, A. Hilger, M. Osenberg, I. Manke, M. Wohlfahrt-Mehrens, V. Schmidt and A. Latz, *J. Electrochem. Soc.*, 2020, **167**, 013546.
58 C.-K. Huang, J. S. Sakamoto, J. Wolfenstine and S. Surampudi, *J. Electrochem. Soc.*, 2000, **147**, 2893.
59 T. L. Kulova, A. M. Skundin, E. A. Nizhnikovskii and A. V. Fesenko, *Russ. J. Electrochem.*, 2006, **42**, 259–262.
60 Y. Ji, Y. Zhang and C.-Y. Wang, *J. Electrochem. Soc.*, 2013, **160**, A636–A649.
61 K. Xu, *Chem. Rev.*, 2014, **114**, 11503–11618.
62 G. Zhu, K. Wen, W. Lv, X. Zhou, Y. Liang, F. Yang, Z. Chen, M. Zou, J. Li, Y. Zhang and W. He, *J. Power Sources*, 2015, **300**, 29–40.

63 A. M. Haregewoin, A. S. Wotango and B. J. Hwang, *Energy Environ. Sci.*, 2016, **9**, 1955–1988.
64 Z. Xu, J. Yang, H. Li, Y. Nuli and J. Wang, *J. Mater. Chem. A*, 2019, **7**, 9432–9446.
65 C. Wang, Y. S. Meng and K. Xu, *J. Electrochem. Soc.*, 2019, **166**, A5184–A5186.
66 L. Liao, P. Zuo, Y. Ma, Y. An, G. Yin and Y. Gao, *Electrochim. Acta*, 2012, **74**, 260–266.
67 L. Liao, X. Cheng, Y. Ma, P. Zuo, W. Fang, G. Yin and Y. Gao, *Electrochim. Acta*, 2013, **87**, 466–472.
68 X. B. Cheng, R. Zhang, C. Z. Zhao and Q. Zhang, *Chem. Rev.*, 2017, **117**, 10403–10473.
69 A. S. Wotango, W. N. Su, A. M. Haregewoin, H. M. Chen, J. H. Cheng, M. H. Lin, C. H. Wang and B. J. Hwang, *ACS Appl. Mater. Interfaces*, 2018, **10**, 25252–25262.
70 J. Wang, F. Lin, H. Jia, J. Yang, C. W. Monroe and Y. Nuli, *Angew. Chem., Int. Ed.*, 2014, **53**, 10099–10104.
71 X. Qi, L. Tao, H. Hahn, C. Schultz, D. R. Gallus, X. Cao, S. Nowak, S. Röser, J. Li, I. Cekic-Laskovic, B. R. Rad and M. Winter, *RSC Adv.*, 2016, **6**, 38342–38349.
72 Y. K. Han, J. Yoo and T. Yim, *J. Mater. Chem. A*, 2015, **3**, 10900–10909.
73 T. Yim and Y. K. Han, *ACS Appl. Mater. Interfaces*, 2017, **9**, 32851–32858.
74 G. Xu, S. Huang, Z. Cui, X. Du, X. Wang, D. Lu, X. Shangguan, J. Ma, P. Han, X. Zhou and G. Cui, *J. Power Sources*, 2019, **416**, 29–36.
75 M. Xu, *Acta Phys. Chim. Sin.*, 2006, **22**, 335–340.
76 L. Liao, T. Fang, X. Zhou, Y. Gao, X. Cheng, L. Zhang and G. Yin, *Solid State Ionics*, 2014, **254**, 27–31.
77 S. Li, X. Li, J. Liu, Z. Shang and X. Cui, *Ionics*, 2015, **21**, 901–907.
78 R. Guo, Y. Che, G. Lan, J. Lan, J. Li, L. Xing, K. Xu, W. Fan, L. Yu and W. Li, *ACS Appl. Mater. Interfaces*, 2019, **11**, 38285–38293.
79 B. Liao, H. Li, M. Xu, L. Xing, Y. Liao, X. Ren, W. Fan, L. Yu, K. Xu and W. Li, *Adv. Energy Mater.*, 2018, **8**, 1800802.
80 J. Shi, N. Ehteshami, J. Ma, H. Zhang, H. Liu, X. Zhang, J. Li and E. Paillard, *J. Power Sources*, 2019, **429**, 67–74.
81 C. Wang, L. Yu, W. Fan, J. Liu, L. Ouyang, L. Yang and M. Zhu, *ACS Appl. Energy Mater.*, 2018, **1**, 2647–2656.
82 K.-E. Kim, J. Y. Jang, I. Park, M.-H. Woo, M.-H. Jeong, W. C. Shin, M. Ue and N.-S. Choi, *Electrochem. Commun.*, 2015, **61**, 121–124.
83 B. Yang, H. Zhang, L. Yu, W. Z. Fan and D. Huang, *Electrochim. Acta*, 2016, **221**, 107–114.
84 Q. Lei, T. Yang, X. Zhao, W. Fan, W. Wang, L. Yu, S. Guo, X. Zuo, R. Zeng and J. Nan, *J. Electroanal. Chem.*, 2019, **846**, 1131412.
85 L. Hamenu, H. S. Lee, M. Latifatu, K. M. Kim, J. Park, Y. G. Baek, J. M. Ko and R. B. Kaner, *Curr. Appl. Phys.*, 2016, **16**, 611–617.
86 J. H. Won, H. S. Lee, L. Hamenu, M. Latifatu, Y. M. Lee, K. M. Kim, J. Oh, W. Il Cho and J. M. Ko, *J. Ind. Eng. Chem.*, 2016, **37**, 325–329.
87 H. Xiang, D. Mei, P. Yan, P. Bhattacharya, S. D. Burton, A. Von Wald Cresce, R. Cao, M. H. Engelhard, M. E. Bowden, Z. Zhu, B. J. Polzin, C. M. Wang, K. Xu, J. G. Zhang and W. Xu, *ACS Appl. Mater. Interfaces*, 2015, **7**, 20687–20695.
88 J. Zheng, P. Yan, R. Cao, H. Xiang, M. H. Engelhard, B. J. Polzin, C. Wang, J. G. Zhang and W. Xu, *ACS Appl. Mater. Interfaces*, 2016, **8**, 5715–5722.
89 Q. Li, S. Jiao, L. Luo, M. S. Ding, J. Zheng, S. S. Cartmell, C. M. Wang, K. Xu, J. G. Zhang and W. Xu, *ACS Appl. Mater. Interfaces*, 2017, **9**, 18826–18835.
90 H.-J. Buysch, *Ullmann's Encyclopedia of Industrial Chemistry*, Wiley-VCH Verlag GmbH & Co. KGaA, Weinheim, Germany, 2000, pp. 565–582.
91 R. Petibon, J. Harlow, D. B. Le and J. R. Dahn, *Electrochim. Acta*, 2015, **154**, 227–234.
92 L. Ma, S. L. Glazier, R. Petibon, J. Xia, J. M. Peters, Q. Liu, J. Allen, R. N. C. Doig and J. R. Dahn, *J. Electrochem. Soc.*, 2017, **164**, A5008–A5018.
93 M. Haruta, T. Okubo, Y. Masuo, S. Yoshida, A. Tomita, T. Takenaka, T. Doi and M. Inaba, *Electrochim. Acta*, 2017, **224**, 186–193.
94 X. Fan, X. Ji, L. Chen, J. Chen, T. Deng, F. Han, J. Yue, N. Piao, R. Wang, X. Zhou, X. Xiao, L. Chen and C. Wang, *Nat. Energy*, 2019, **4**, 882–890.
95 M. J. Piernas-Muñoz, S. E. Trask, A. R. Dunlop, E. Lee and I. Bloom, *J. Power Sources*, 2019, **441**, 227080.
96 M. C. Smart, B. V. Ratnakumar, S. Surampudi, Y. Wang, X. Zhang, S. G. Greenbaum, A. Hightower, C. C. Ahn and B. Fultz, *J. Electrochem. Soc.*, 1999, **146**, 3963.
97 M. C. Smart, B. V. Ratnakumar and S. Surampudi, *J. Electrochem. Soc.*, 2002, **149**, A361.
98 Y. Ein-Eli, S. R. Thomas, R. Chadha, T. J. Blakley and V. R. Koch, *J. Electrochem. Soc.*, 1997, **144**, 823.
99 M. C. Smart, B. V. Ratnakumar, K. B. Chin and L. D. Whitcanack, *J. Electrochem. Soc.*, 2010, **157**, A1361.
100 K. A. Smith, M. C. Smart, G. K. S. Prakash and B. V. Ratnakumar, *ECS Trans.*, 2008, **11**, 91–98.
101 W. Lu, K. Xie, Z. Chen, S. Xiong, Y. Pan and C. Zheng, *J. Power Sources*, 2015, **274**, 676–684.
102 X. Ma, R. S. Arumugam, L. Ma, E. Logan, E. Tonita, J. Xia, R. Petibon, S. Kohn and J. R. Dahn, *J. Electrochem. Soc.*, 2017, **164**, A3556–A3562.
103 X. Ma, J. Li, S. L. Glazier, L. Ma, K. L. Gering and J. R. Dahn, *Electrochim. Acta*, 2018, **270**, 215–223.
104 J.-P. Jones, M. C. Smart, F. C. Krause and R. V. Bugga, *J. Electrochem. Soc.*, 2020, **167**, 020536.
105 E. R. Logan, E. M. Tonita, K. L. Gering, J. Li, X. Ma, L. Y. Beaulieu and J. R. Dahn, *J. Electrochem. Soc.*, 2018, **165**, A21–A30.
106 K. Chen, Z. Yu, S. Deng, Q. Wu, J. Zou and X. Zeng, *J. Power Sources*, 2015, **278**, 411–419.
107 X. Dong, Z. Guo, Z. Guo, Y. Wang and Y. Xia, *Joule*, 2018, **2**, 902–913.
108 J. F. Côté, D. Brouillette, J. E. Desnoyers, J. F. Rouleau, J. M. St-Arnaud and G. Perron, *J. Solution Chem.*, 1996, **25**, 1163–1173.

109 M. L. Lazar and B. L. Lucht, *J. Electrochem. Soc.*, 2015, **162**, A928–A934.
110 P. Shi, S. Fang, J. Huang, D. Luo, L. Yang and S. I. Hirano, *J. Mater. Chem. A*, 2017, **5**, 19982–19990.
111 Y. Gu, S. Fang, L. Yang and S. Ichi Hirano, *Electrochim. Acta*, 2021, **394**, 139120.
112 H. F. Xiang, B. Yin, H. Wang, H. W. Lin, X. W. Ge, S. Xie and C. H. Chen, *Electrochim. Acta*, 2010, **55**, 5204–5209.
113 I. A. Shkrob, T. W. Marin, Y. Zhu and D. P. Abraham, *J. Phys. Chem. C*, 2014, **118**, 19661–19671.
114 M. Kunze, S. Jeong, G. B. Appetecchi, M. Schönhoff, M. Winter and S. Passerini, *Electrochim. Acta*, 2012, **82**, 69–74.
115 F. Wohde, M. Balabajew and B. Roling, *J. Electrochem. Soc.*, 2016, **163**, A714–A721.
116 M. Yamagata, Y. Matsui, T. Sugimoto, M. Kikuta, T. Higashizaki, M. Kono and M. Ishikawa, *J. Power Sources*, 2013, **227**, 60–64.
117 W. Wang, T. Yang, S. Li, W. Fan, X. Zhao, C. Fan, L. Yu, S. Zhou, X. Zuo, R. Zeng and J. Nan, *Electrochim. Acta*, 2019, **317**, 146–154.
118 K. Oldiges, J. Michalowsky, M. Grünebaum, N. von Aspern, I. Cekic-Laskovic, J. Smiatek, M. Winter and G. Brunklaus, *J. Power Sources*, 2019, **437**, 226881.
119 C. S. Rustomji, Y. Yang, T. K. Kim, J. Mac, Y. J. Kim, E. Caldwell, H. Chung and Y. S. Meng, *Science*, 2017, **356**, eaal4263.
120 Y. Yang, M. Daniel, Y. Yin, C. S. Rustomji, Y. Yang, D. M. Davies, Y. Yin, O. Borodin, J. Z. Lee, C. S. Rustomji and Y. S. Meng, *Joule*, 2019, **3**, 1986–2000.
121 Y. Yang, Y. Yin, D. M. Davies, M. Zhang, M. Mayer, Y. Zhang, E. S. Sablina, S. Wang, J. Z. Lee, O. Borodin, C. S. Rustomji and Y. S. Meng, *Energy Environ. Sci.*, 2020, **13**, 2209–2219.
122 S. Zhang, K. Xu and T. Jow, *Electrochem. Commun.*, 2002, **4**, 928–932.
123 S. S. Zhang, K. Xu and T. R. Jow, *J. Solid State Electrochem.*, 2003, **7**, 147–151.
124 K. Xu, S. S. Zhang, U. Lee, J. L. Allen and T. R. Jow, *J. Power Sources*, 2005, **146**, 79–85.
125 T. R. Jow, M. S. Ding, K. Xu, S. S. Zhang, J. L. Allen, K. Amine and G. L. Henriksen, *J. Power Sources*, 2003, **119–121**, 343–348.
126 K. Xu, S. Zhang and R. Jow, *US Pat.*, US8632918B2, 2014.
127 K. Xu, *J. Electrochem. Soc.*, 2008, **155**, A733.
128 S. Shui Zhang, *Electrochem. Commun.*, 2006, **8**, 1423–1428.
129 H. Zhou, K. Xiao and J. Li, *J. Power Sources*, 2016, **302**, 274–282.
130 B. K. Mandal, A. K. Padhi, Z. Shi, S. Chakraborty and R. Filler, *J. Power Sources*, 2006, **162**, 690–695.
131 J. Chen, J. Vatamanu, L. Xing, O. Borodin, H. Chen, X. Guan, X. Liu, K. Xu and W. Li, *Adv. Energy Mater.*, 2020, **10**, 1902654.
132 M. Becker, R. S. Kühnel and C. Battaglia, *Chem. Commun.*, 2019, **55**, 12032–12035.
133 H. I. Kim, E. Shin, S. H. Kim, K. M. Lee, J. Park, S. J. Kang, S. So, K. C. Roh, S. K. Kwak and S. Y. Lee, *Energy Storage Mater.*, 2021, **36**, 222–228.
134 S.-T. Myung, Y. Hitoshi and Y.-K. Sun, *J. Mater. Chem.*, 2011, **21**, 9891.
135 X. Zuo, J. Zhu, P. Müller-Buschbaum and Y.-J. Cheng, *Nano Energy*, 2017, **31**, 113–143.
136 G. G. Eshetu and E. Figgemeier, *ChemSusChem*, 2019, **12**, 2515–2539.
137 H. Zhao, W. Yuan and G. Liu, *Nano Today*, 2015, **10**, 193–212.
138 U. S. Kasavajjula and C. Wang, *Indian J. Chem. - Sect. A Inorganic, Phys. Theor. Anal. Chem.*, 2005, **44**, 975–982.
139 E. Markevich, G. Salitra and D. Aurbach, *J. Electrochem. Soc.*, 2016, **163**, A2407–A2412.
140 T. Subburaj, W. Brevet, F. Farmakis, D. Tsiplakides, S. Balomenou, N. Strataki, C. Elmasides, B. Samaniego and M. Nestoridi, *Electrochim. Acta*, 2020, **354**, 0–8.
141 K. Richter, T. Waldmann, N. Paul, N. Jobst, R. G. Scurtu, M. Hofmann, R. Gilles and M. Wohlfahrt-Mehrens, *ChemSusChem*, 2020, **13**, 529–538.
142 Y. Yan, L. Ben, Y. Zhan and X. Huang, *Electrochim. Acta*, 2016, **187**, 186–192.
143 D. H. C. Wong, J. L. Thelen, Y. Fu, D. Devaux, A. A. Pandya, V. S. Battaglia, N. P. Balsara and J. M. DeSimone, *Proc. Natl. Acad. Sci. U. S. A.*, 2014, **111**, 3327–3331.
144 X. Ren, S. Chen, H. Lee, D. Mei, M. H. Engelhard, S. D. Burton, W. Zhao, J. Zheng, Q. Li, M. S. Ding, M. Schroeder, J. Alvarado, K. Xu, Y. S. Meng, J. Liu, J.-G. Zhang and W. Xu, *Chem*, 2018, **4**, 1877–1892.
145 Y. Zhao, C. Fang, G. Zhang, D. Hubble, A. Nallapaneni, C. Zhu, Z. Zhao, Z. Liu, J. Lau, Y. Fu and G. Liu, *Front. Chem.*, 2020, **8**, 1–9.

